https://doi.org/10.5194/egusphere-2026-2659
Preprint. Discussion started: 29 May 2026


# Elevated Aerosol Layers within the Daytime Mixed Layer Over Ecologically Sensitive Areas of Northwest China: Diurnal Variation, Formation Mechanisms and Regional Effects

Zikai Lin [a], Tian Zhou [a,*], Zhengpeng Li [a], Yonghong Gu [a], Dongsheng Wu [a], Ping Zhou [c], Keyu Zhang [a], Qili Gao [a], Xingran Li [a], Zhongwei Huang [a,b], Jianrong Bi [a,b], Lili Yang[d], Lina Wang[d]

[a] Key Laboratory for Semi-Arid Climate Change of the Ministry of Education, College of Atmospheric Sciences, Lanzhou University, Lanzhou 730000, China.
[b] Collaborative Innovation Center for Western Ecological Safety, Lanzhou University, Lanzhou, 730000, China.
[c] School of Atmospheric Sciences, Sun Yat-sen University, Zhuhai, Guangdong 519082, China
[d] Gansu Province Environmental Monitoring Center, Lanzhou 730000, China.

Corresponding author: zhoutian@lzu.edu.cn

https://doi.org/10.5194/egusphere-2026-2659
Preprint. Discussion started: 29 May 2026


**Abstract.** The cyclic processes of aerosol evolution have a profound impact on regional climate, water resources and ecosystems. However, studies on diurnal variations of aerosol vertical distribution in typical ecologically sensitive areas remain scarce due to limited availability of high-resolution profiles. This study first identifies the elevated aerosol layer (EAL) within the daytime mixed layer over the Hexi Corridor, northwest China, defined as a high-concentration layer above the surface but within the mixed layer. Based on intensive observation campaigns conducted in 2010 and 2012, we analyze the diurnal variation, formation mechanisms, air quality and radiative effects of EALs. The results show that EALs frequently occur at altitudes of 0.6–2km during daytime. Excluding dust storms, the occurrence frequencies reaches 81% (37%) in Dunhuang (Minqin) region , dominated by dust aerosol (anthropogenic pollutants). Driven by a thermodynamic coupling effect characterized by positive anomalies in potential temperature and negative anomalies in relative humidity, aerosols accumulate at the bottom of the stable stratification. Thus, a simplified conceptual model for prediction is proposed. The peak PM10 concentration within EAL (203.3±106.6μg/m³) at ~1.2km is five times higher than that at surface (40.8±30.4μg/m³). Furthermore, the EALs enhance the atmospheric shortwave heating rate (up to 0.7K/day), and form a daily-scale heating pump that may accelerate snowmelt/glacier retreat in the region. These findings suggest that the aerosol vertical evolution should receive greater consideration in air pollution prevention, ecosystem protection, water resource management, and wind/solar energy utilization in ecologically sensitive areas-particularly over complex terrains-rather than focusing solely on surface air pollution.

https://doi.org/10.5194/egusphere-2026-2659
Preprint. Discussion started: 29 May 2026


## 1. Introduction

Aerosols exert significant environmental and climatic impacts. Aerosol properties exhibit substantial variability across temporal and spatial scales; it is crucial to accurately characterise the three-dimensional spatiotemporal distribution of aerosols (Park and Allen, 2015; Manavi et al., 2025). The vertical distribution of aerosols is a primary factor modulating their radiative effects (Sun et al., 2018; Guo et al., 2022; Che et al., 2024; Derepentigny, 2024; Huang et al., 2014), as it directly determines their interactions with solar and outgoing longwave radiation (Liu et al., 2019; Fountoulakis et al., 2022). It also governs the deposition of light-absorbing aerosols such as dust and black carbon in high-mountain snowpacks, thereby regulating snow albedo reduction and accelerating glacial snowmelt in high-altitude regions (Sarangi et al., 2020). In addition, the vertical distribution of aerosols serves as an important indicator for assessing regional pollution levels and tracing emission sources (Huige et al., 2021; Pace et al., 2015). Further, it can influence atmospheric stability, thereby affecting the development of turbulence and cloud formation (Petrovic et al., 2017; Li et al., 2021; Liang et al., 2022; Su et al., 2020b).

To date, substantial progress has been made in understanding aerosol diurnal variations, which can generally be classified into two categories: the diurnal cycle of ground-level air pollutants (Jia et al., 2018; Huszar et al., 2020; Shivkumar et al., 2022; Wang et al., 2021; Diya et al., 2024), and the diurnal variation of column-integrated aerosol optical properties (Reddy et al., 2015; Smirnov et al., 2002; Song et al., 2018). The vertical distribution of aerosols establishes a strong linkage between ground-level aerosol concentrations and column-integrated aerosol properties. It exhibits pronounced diurnal variability, driven by synoptic-scale systems and atmospheric boundary layer (ABL) evolution. Compared with the abundance of ground-level observations and column-integrated aerosol properties measurements, continuous, high-resolution observations of aerosol vertical distribution remain scarce. Aerosols are primarily concentrated within the ABL; the diurnal cycle of the ABL constitutes the fundamental dynamical regime and dominant framework governing the diurnal evolution of aerosol vertical structure (Hara et al., 2022; Su et al., 2020c; Zhang et al., 2023c; Song et al., 2024). Local circulations, such as sea–land breezes and mountain–valley winds, drive diurnally reversing vertical transport, thereby governing aerosol layering, accumulation, and migration through modulation of vertical diffusion and transport processes throughout the day (Zhang et al., 2023a; Zhang et al., 2023b;

https://doi.org/10.5194/egusphere-2026-2659
Preprint. Discussion started: 29 May 2026


Boselli et al., 2009; Boselli et al., 2004). Inversion layers form a stable stratification structure whose diurnal evolution directly controls the intensity of atmospheric vertical exchange and the extent of aerosol trapping (Li et al., 2022; Liu et al., 2024; Parajuli et al., 2020), while turbulent mixing serves as the primary physical mechanism governing aerosol vertical transport and redistribution (Li et al., 2019; Noh et al., 2013). Meanwhile, diurnal variability in anthropogenic emissions intensity, as well as the altitude and strength of long-range transport, significantly influences aerosol vertical structure (Du et al., 2020; Yim and Huang, 2023; Cheng et al., 2020; Xiang et al., 2021). In addition, the interactions between aerosol and boundary layer, particularly the radiative effects of absorbing particles, can induce positive feedback mechanisms that alter stratification stability and suppress boundary layer development (Prasad et al., 2022; Su et al., 2020c), thereby modulating aerosol vertical structure. Although existing studies have achieved a relatively systematic understanding, significant gaps remain in elucidating the driving mechanisms of diurnal variations in aerosol vertical structure across different climatic zones and underlying surface conditions, primarily due to the scarcity of long-term, continuous, high spatiotemporal resolution profile measurements.

The Hexi Corridor is located adjacent to the northeastern margin of the Qinghai–Tibet Plateau and the surrounding deserts and Gobi regions. It serves as an ecological barrier in the arid and semi-arid regions of Northwest China. On the one hand, it strongly restricts the geographical expansion of deserts, forming the first line of defense against sand encroachment and desertification in inland Northwest China. On the other hand, it plays a critical role in protecting the scarce and valuable water resources of Northwest China, serving as a core lifeline for maintaining ecological balance in arid regions and ensuring water security for both human livelihoods and ecosystems. As the source region of several inland rivers, the Qilian Mountains within the Hexi Corridor act as a key regulator of regional water availability and ecosystem sustainability through orographic precipitation and glacial meltwater supply. Absorbing aerosols, such as dust and black carbon, when transported and deposited onto glaciers and snow cover in high-mountain regions, accelerate ablation by reducing surface albedo, thereby directly impacting water resource storage and security (Ramanathan et al., 2007; Sarangi et al., 2020; Hou et al., 2018). Additionally, aerosols significantly influence the microphysical processes and precipitation efficiency of mountainous clouds, potentially altering local precipitation patterns (Chen et al., 2011; Jian et al., 2025; Zhao et al., 2024). Therefore, conducting aerosol research in such regions is of great significance for environmental sustainability and ecological protection. In addition, significant efforts

https://doi.org/10.5194/egusphere-2026-2659
Preprint. Discussion started: 29 May 2026


have been made in recent years to strengthen the construction of a regional three-dimensional observation network over the Hexi Corridor region (Huang et al., 2024; Yang et al., 2025); however, the diurnal cycle of aerosol vertical distribution and its regional impacts have not yet received sufficient attention.

In summary, to further explore the potential of the three-dimensional observation network in supporting regional ecological sustainability, this study aims to elucidate the diurnal variation of aerosol vertical distribution, its potential controlling mechanisms, and its radiative and environmental effects, based on two intensive observation periods conducted in 2010 at Minqin and in 2012 at Dunhuang in the Hexi Corridor region. Section 2 introduces the study sites and methodologies. In Section 3, analyses the characteristics of diurnal variation in aerosol vertical distribution, explores the underlying mechanisms, and evaluates the associated radiative and environmental effects. Finally, the conclusions are presented in Section 4.

## 2. Data and methods

### 2.1 Field campaigns

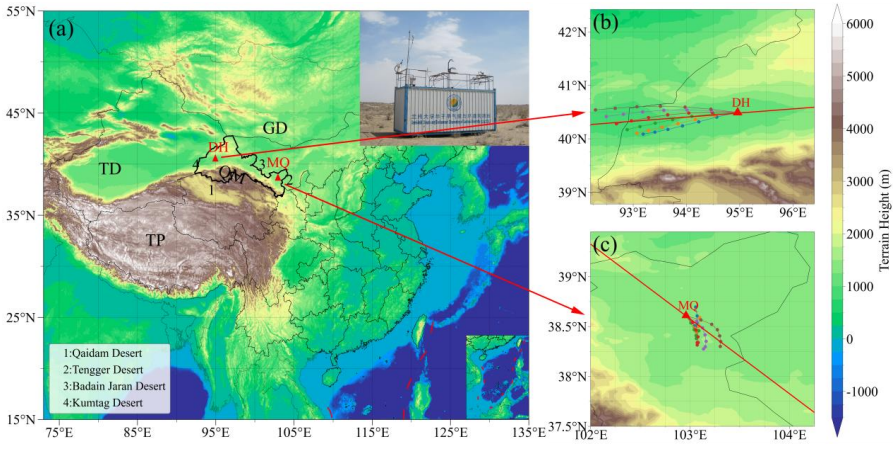


**Fig. 1. Observation locations of Dunhuang (DH) and Minqin (MQ), their surrounding areas, and photographs of the mobile facilities. HYSPLIT backward trajectories are shown, and the red lines in the right panel represent the selected cases in Dunhuang and Minqin.**

This study utilises data from intensive field observations conducted using the mobile facilities of the Semi-Arid Climate and Environment Observatory of Lanzhou University (SACOL) (Fig. 1) at Minqin (38.607°N, 102.959°E, 1373 m a.s.l) from April to June 2010 and at Dunhuang (40.492°N,

https://doi.org/10.5194/egusphere-2026-2659
Preprint. Discussion started: 29 May 2026


94.955°E, 1061 m a.s.l) from April to June 2012 in the Hexi Corridor region. The mobile facilities were equipped with a suite of instruments to measure key atmospheric parameters, including atmospheric radiation, aerosol scattering and absorption coefficients, aerosol optical depth, mass concentration, and aerosol vertical distribution. Dunhuang is located at the westernmost end of the Hexi Corridor, adjacent to the Kumtag Desert to the west, approximately 450 km downwind of the Taklimakan Desert, bordering the Badain Jaran Desert to the east, and close to the Qilian Mountains to the south. Owing to its unique geographical location, distinctive underlying surface characteristics, extreme aridity, and strong prevailing winds, dust storms frequently occur in this region during spring. The observation site was located approximately 45 km northeast of Dunhuang City and was surrounded by farmland, Gobi Desert, and saline–alkali land. Minqin is located in the northeastern part of the Hexi Corridor, at the convergence zone of the Badain Jaran and Tengger Deserts, and is close to the Qilian Mountains to the southwest, making it highly susceptible to aeolian processes. The region is characterised by a temperate continental hyper-arid climate. Dust events also occur frequently during springtime. The observation site was surrounded by sand dunes interspersed with small patches of farmland, representing a typical desert–oasis transition zone (Zhou et al., 2018).

### 2.2 Observation Instruments

#### 2.2.1 Micro-Pulse Lidar (MPL)

The micro-pulse lidar (MPL-4B; manufactured by Sigma Space Corporation) is a safe, compact, and maintenance-free system with a wavelength of 527 nm, a temporal resolution of 1 min, a spatial resolution of 30 m, an emission energy of 6–8 μJ, a pulse repetition frequency of 2500 Hz and a blind zone of 600 m. MPL observations are corrected and preprocessed using the algorithm proposed in previous studies (Xie et al., 2017; Zhou et al., 2018). Subsequently, aerosol optical properties, including the extinction coefficient, backscattering coefficient, particle depolarisation ratio, cloud top and base heights, and cloud thermodynamic phase, are retrieved.

To identify elevated aerosol layers in this study, the following discrimination procedure was adopted: observations between 13:00 and 21:00 Beijing Time (the period of frequent occurrence of elevated aerosol layers) were selected for analysis; following the method of (Zhou et al., 2021; Zhou et al., 2018), a depolarisation ratio greater than 0.20 was used as the threshold for identifying dust aerosols. For both sites, if the proportion of dust aerosol observations exceeds 50% on a given day, the

https://doi.org/10.5194/egusphere-2026-2659
Preprint. Discussion started: 29 May 2026


day is classified as a dust event and subsequently excluded. This classification is based on the gradient characteristics of the vertical profiles. If a continuous positive gradient is observed and the corresponding proportion of observations exceeds 20%, an elevated aerosol layer is considered to be present. The selection of the aforementioned thresholds is based on the stability of event classification. By systematically evaluating different threshold combinations and analysing the variability of the corresponding classification results, the optimal combination—defined as that which minimises fluctuations and maximises consistency—is ultimately selected as the determination criterion.

Additionally, to quantify the mass concentration of elevated aerosol layers at higher altitudes, an empirical relationship was established between ground-level PM10 concentration observations and the lowest two sampling bins (~600m) in the averaged profiles of the aerosol extinction coefficient. Statistical analysis during the experimental period revealed a significant correlation ($R = 0.8$, $n = 4357$) between PM10 mass concentration and the aerosol extinction coefficient ($\alpha$) (not shown here), yielding the following regression equation:

$$PM_{10} = 914.65 \times \alpha - 56.26 \quad (1)$$

#### 2.2.2 Other Data and Tools

The aerosol optical depth (AOD) and Ångström exponent (AE) used in this study were retrieved from a Cimel CE-318 sun photometer, a passive remote-sensing instrument manufactured by CIMEL (France), designed to measure both direct solar and diffuse sky radiation. This instrument serves as the standard platform within the AERONET (Aerosol Robotic Network) observation network (Holben et al., 1998). The CE-318 is equipped with multiple spectral channels (e.g. 440, 670, 870, 936, and 1020 nm) and performs automated sun-tracking and sky-scanning measurements at 15 min intervals. Single-scattering albedo (SSA) and the asymmetry factor (ASY) were also retrieved from the AERONET database (Marsli et al.). The SSA and ASY represent statistically averaged aerosol optical properties derived from Level 1.5 AERONET products based on observations at the Dunhuang and Minqin sites.

Ground-level meteorological parameters, including air temperature, relative humidity, air pressure, wind speed, and wind direction, were measured using an automatic meteorological station (model WXT520; Vaisala, Vantaa, Finland). The instrument was mounted on top of a mobile platform at an approximate height of 4 m above ground level. Raw data averaged at 1 min intervals were used in this

https://doi.org/10.5194/egusphere-2026-2659
Preprint. Discussion started: 29 May 2026


study.

PM10 mass concentration was continuously monitored using an ambient particulate monitor with a resolution of 0.1 μg/m3. This instrument operates based on the principle of a tapered element oscillating microbalance (TEOM; model RP1400a, Rupprecht and Patashnick Company) with a flow rate of 16.7 L/min (Patashnick and And Rupprecht, 1991). In this study, instances in which negative PM10 concentration values occurred due to heating of the sampling stream (50 °C) and the partial loss of volatile and semi-volatile aerosol compounds were excluded. These negative values accounted for less than 1% of the total dataset (Zhou et al., 2018; Bi et al., 2017).

Meteorological conditions and the formation mechanisms of elevated aerosol layers were characterised and analysed using the ERA5 reanalysis dataset (available at https://cds.climate.copernicus.eu/), a high-resolution global atmospheric reanalysis product developed by the European Centre for Medium-Range Weather Forecasts (ECMWF). This comprehensive dataset, spanning from 1979 to the present, with an hourly temporal resolution (1 h) and a spatial resolution of 0.25° × 0.25°, provides 37 vertical pressure levels ranging from 1000 to 1 hPa and includes key meteorological parameters such as temperature, pressure, wind fields, relative humidity, and cloud cover (Nogueira, 2020; Albergel et al., 2018).

To trace air mass source regions, the Hybrid Single-Particle Lagrangian Integrated Trajectory (HYSPLIT) model was employed. This modelling system, developed by the Air Resources Laboratory (ARL) of the National Oceanic and Atmospheric Administration (NOAA), is widely used to simulate the transport and dispersion of aerosols, gases, and other atmospheric constituents. It integrates the advantages of both Lagrangian particle models and Eulerian grid-based models, thereby enabling the simulation of atmospheric transport processes across a wide range of spatial scales, from local to global (Stein et al., 2015).

To quantify the radiative effects of elevated aerosol layers, this study employed the Santa Barbara DISORT Atmospheric Radiative Transfer (SBDART) model, which is grounded in well-established radiative transfer theory and is widely used in remote sensing applications and atmospheric energy budget analyses (Ricchiazzi et al., 1998). In this study, the model input parameters were constrained using multiple observational datasets to improve the accuracy of radiative forcing simulations. These inputs include shortwave (0.3–2.8 μm) radiative flux, surface albedo, and site location data obtained from an automatic meteorological station. Additional aerosol optical properties, including aerosol

https://doi.org/10.5194/egusphere-2026-2659
Preprint. Discussion started: 29 May 2026


optical depth and Ångström exponent, along with water vapour parameters, were retrieved from a CE-318 sun photometer. Aerosol and atmospheric vertical profiles, including air density, specific humidity, temperature, and ozone, were derived from lidar observations and reanalysis datasets (ERA5 and MERRA2), with the latter additionally providing hourly atmospheric profiles. Furthermore, total column ozone was retrieved from the Ozone Monitoring Instrument. These dynamically constrained inputs resulted in excellent model performance, as evidenced by the high coefficients of determination between simulated and observed radiation components. Specifically, the coefficients of determination ($R^2$) between simulated and observed direct and diffuse radiation were 0.999 and 0.982, respectively (not shown here), thereby confirming the robustness of the model configuration. (Li et al., 2025)

Here, the shortwave radiative forcing (SRF) and shortwave heating rate are calculated under clear-sky conditions (Jangid et al., 2024) and can be expressed as follows:

$$\triangle F = F\downarrow - F\uparrow \quad (2)$$

where $\triangle F$ denotes the net downward radiative flux.

$$SRF(TOA) = \triangle F^{aerosol}(TOA) - \triangle F^{no}(TOA) \quad (3)$$

$$SRF(SFC) = \triangle F^{aerosol}(SFC) - \triangle F^{no}(SFC) \quad (4)$$

$$SRF(ATM) = SRF(TOA) - SRF(SFC) \quad (5)$$

TOA, SFC, and ATM denote the top of the atmosphere, the surface, and the atmospheric column, respectively. The labels “aerosol” and “no” indicate conditions with and without aerosols, respectively.

$$ASHR(z) = SHR(z)^{aerosol} - SHR(z)^{no} \quad (6)$$

where ASHR(z) denotes the aerosol shortwave heating rate at height z.

## 3. Results and discussion

### 3.1 Overview of field observations

https://doi.org/10.5194/egusphere-2026-2659
Preprint. Discussion started: 29 May 2026


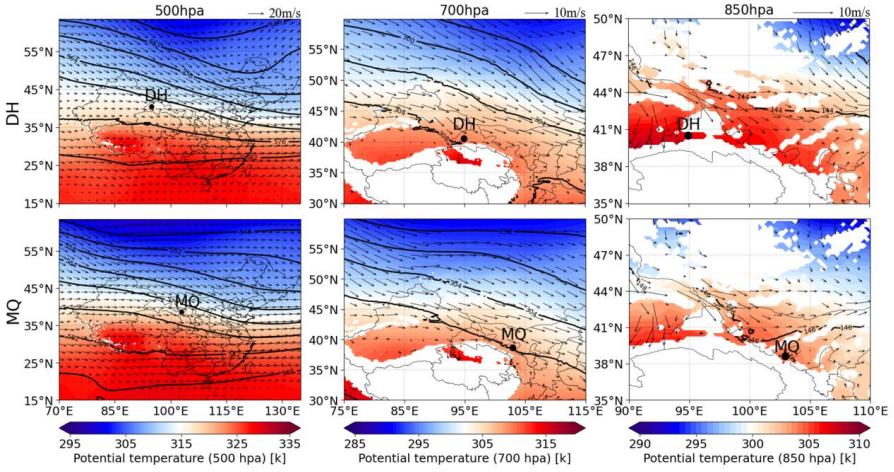


**Fig. 2. Mean meteorological fields during the two intensive observation periods (Dunhuang: 1 April–10 June 2012; Minqin: 21 April–15 June 2010), with geopotential height contours. The white regions indicate elevated mountainous terrain.**

First, the meteorological background during both intensive observation periods is shown in Fig. 2. It can be seen that both sites are influenced by the westerlies at the 500 hPa level. At the 700 and 850 hPa levels, the influence of complex topography becomes evident. The wind direction at both sites aligns with the orientation of the Qilian Mountains, with airflow predominantly from northwest to southeast. Areas surrounding the Qilian Mountains and the Hexi Corridor exhibit high potential temperatures, indicating an unstable atmospheric state that is favourable for the enhancement of vertical motion (Zhao et al., 2005). At the Dunhuang site, wind speeds are relatively high, generally exhibiting a north-to-south flow pattern. In contrast, wind speeds at the Minqin site are lower, and the site is located on the western flank of an anticyclone within a low-pressure centre, leading to convergent ascending motion (Wang et al., 2024). Therefore, based on the mean meteorological fields, atmospheric conditions over the Hexi Corridor region during the entire experimental period were relatively unstable, with potential upward motion, providing a favourable meteorological background for the vertical transport of aerosols.

https://doi.org/10.5194/egusphere-2026-2659
Preprint. Discussion started: 29 May 2026


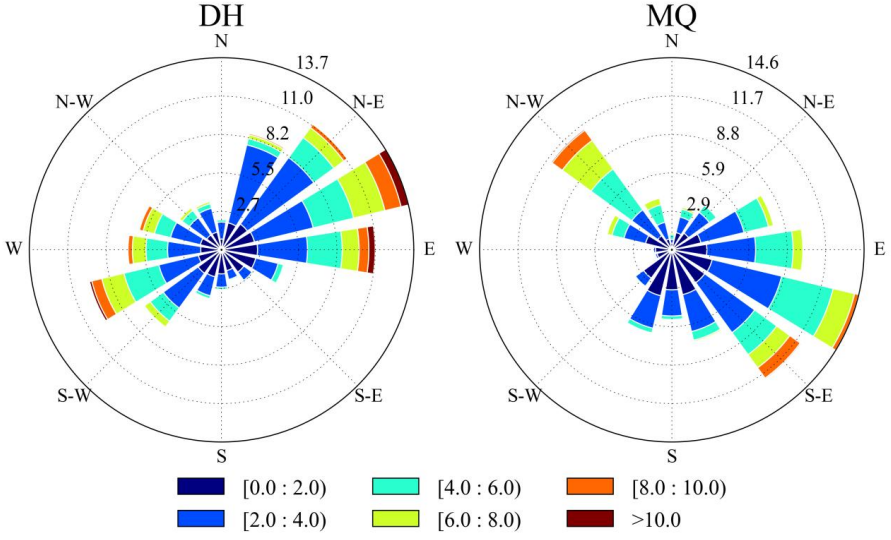


**Fig. 3. Surface wind speed and wind direction during the intensive observation periods at Dunhuang from 1 April to 10 June 2012 (left) and Minqin from 21 April to 15 June 2010 (right).**

The complex mountainous terrain also generates distinct patterns in the local distribution of wind speed and direction. Concurrently, the extensive surrounding desert surfaces serve as major aerosol sources, profoundly influencing local aerosol composition and speciation. As shown in Fig. 3, northeasterly and southwesterly winds prevail at the Dunhuang site, with an average wind speed of 3.5 m/s. Aerosols are likely derived mainly from dust originating from the Gobi Desert and sandy areas surrounding the observation site, as well as from the Kumtag Desert to the southwest (Luo et al., 2022). At the Minqin site, southeasterly winds dominate, with an average wind speed of 3.2 m/s. Aerosols are likely primarily derived from dust originating from the Tengger Desert to the southeast or the Badain Jaran Desert to the northwest (Yang et al., 2024). The prevailing wind directions of both sites not only exhibit higher frequencies of occurrence but are also associated with relatively higher wind speeds, which are closely related to wind channelling effects induced by topographic undulations (Dang et al., 2024).

https://doi.org/10.5194/egusphere-2026-2659
Preprint. Discussion started: 29 May 2026


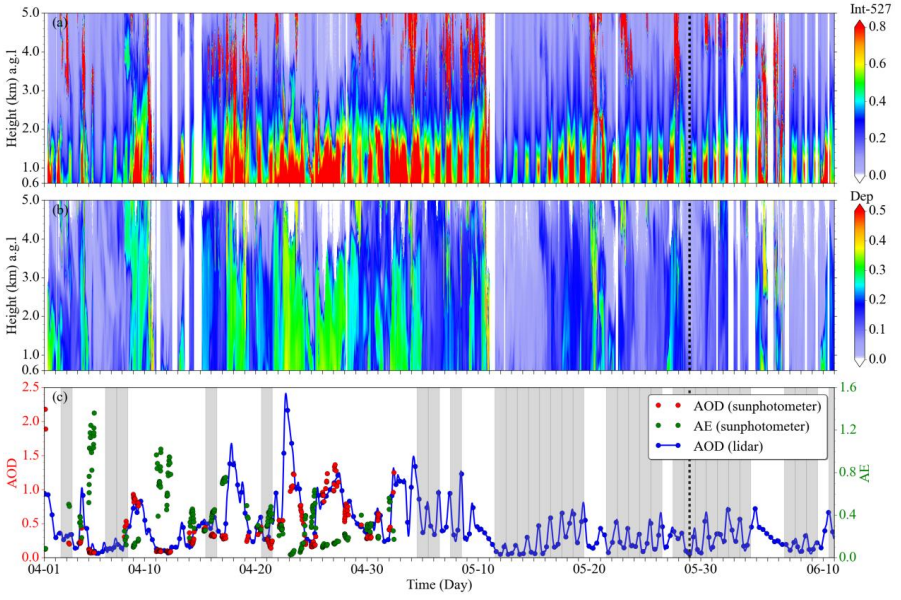


**Fig. 4. Time series of observations obtained from a micro-pulse lidar (MPL) and a sun photometer during the intensive observation period at Dunhuang in 2012. Time–height cross-sections of (a) normalised relative backscatter (NRB) and (b) linear volume depolarisation ratio (Dep) derived from MPL observations. (c) Time series of aerosol optical depth (AOD) retrieved from AERONET at 500 nm (red dots) and from MPL at 527 nm, along with the Ångström exponent (AE) at 440–870 nm (green dots). All identified elevated aerosol layers are indicated by shaded regions, and the representative case selected for detailed discussion is highlighted with black dashed lines.**

The evolution of aerosol vertical distribution and column properties over Dunhuang is presented in Fig. 4. In Fig. 4a–b, high normalised relative backscatter and high depolarisation ratios indicate elevated dust aerosol loading, including dust events (Zhou et al., 2021; Zhou et al., 2024). Dust events frequently occurred before 4 May. Thereafter, although dust events still occurred, their intensity and duration were significantly reduced. Instead, more distinct diurnal variations in aerosol vertical distribution are observed. These vertical distributions exhibit high normalised relative backscatter but a broader range of depolarisation ratios, indicating that not all observations correspond to dust particles. The maximum normalised relative backscatter is located at approximately 1 km, indicating the presence of elevated aerosol layers. According to the method described in Section 2.2.1, the occurrence frequency of elevated aerosol layers is approximately 81% during the experimental period, excluding dust events. As shown in Fig. 4c, most of these events occurred after 10 May. Owing to the limited availability of CE-318 observations during the experiment, aerosol column properties were derived by column-integrating the aerosol extinction coefficient retrieved from lidar to calculate AOD, following

https://doi.org/10.5194/egusphere-2026-2659
Preprint. Discussion started: 29 May 2026


the approach used in our previous study (Zhou et al., 2021). The correlation coefficient between the two AOD datasets is 0.86, with a root-mean-square error of 0.18. This indicates the reliability of AOD retrieved from lidar in the absence of CE-318 observations. AOD values during elevated aerosol layer episodes were considerably lower than those during dust events, and the variability in AOD during each episode remained relatively consistent. To a certain extent, the depolarisation ratio can characterise the coarse- and fine-mode particle fractions. For example, on 5 and 11 April, lower depolarisation ratios correspond to higher Ångström exponent (AE) values, indicating that the elevated aerosol layers contain a larger fraction of fine-mode particles (Huang et al., 2025). Similar patterns are observed on 14 May and 7–8 June. However, relatively high depolarisation ratios observed on 18 and 23 May, indicate the presence of mixed aerosol types containing dust components.

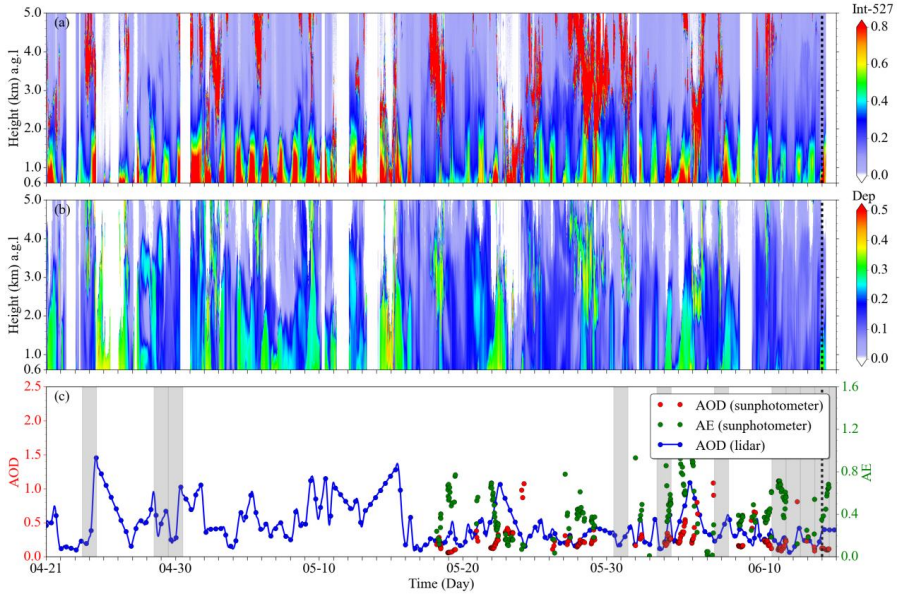


**Fig. 5. Same as Fig.4, but for Minqin in 2010.**

Similarly, Fig. 5 provides an overview of aerosol evolution over Minqin. A notable contrast is observed compared with Dunhuang, despite the consistency of observation season. High dust loading was also observed at Minqin; however, dust events were less intense but more frequent and temporally dispersed than those at Dunhuang, occurring intermittently throughout the experiment, with the highest frequency in May. In contrast to the lower values observed at Dunhuang, depolarisation ratios remained consistently high at Minqin. This indicates that concentrations of coarse-mode particles (e.g., dust aerosols) were comparatively higher at Minqin during the observation period. For elevated aerosol

https://doi.org/10.5194/egusphere-2026-2659
Preprint. Discussion started: 29 May 2026


310 layers (excluding dust days), the occurrence frequency at Minqin was only 37%, with such events primarily concentrated in June (Fig. 5c). Moreover, the overall height of elevated aerosol layers at Minqin was lower than that at Dunhuang, and their intensity was also weaker. The correlation coefficient between AOD values retrieved by lidar and CE-318 was 0.70, with a root-mean-square error of 0.06. Notably, the AE was relatively high in June, when elevated aerosol layer events were frequent.
315 In particular, the mean AE reached 0.6 during elevated aerosol layer events, indicating the dominance of fine-mode aerosols during this period.

### 3.2 Diurnal variation

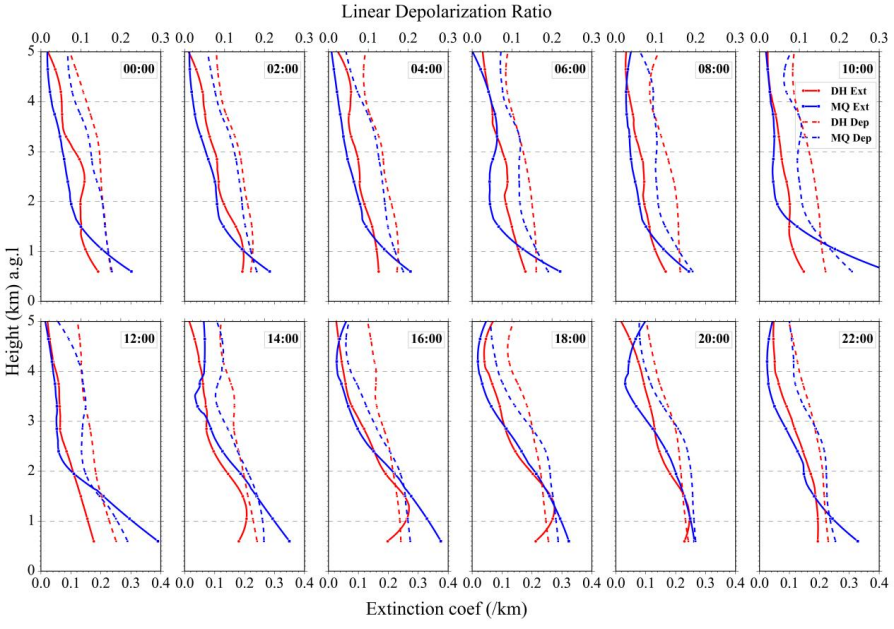


**Fig. 6 Hourly averaged vertical profiles of aerosol extinction coefficient (solid lines) and linear**
320 **volume depolarisation ratio (dashed lines) during the experimental periods at Dunhuang (red lines) and Minqin (blue lines).**

To provide a more intuitive representation of the diurnal variations in aerosol vertical structure at the two sites, hourly averaged extinction coefficient profiles at specific times during the experimental periods are presented in Fig. 6. Within the vertical range of 0.6–2 km a.g.l. at Dunhuang, the aerosol
325 extinction coefficient exhibited a weak decreasing trend from 22:00 to 12:00 the following day. However, from 14:00 to 20:00, a distinct nose-shaped structure appeared, with a peak near 1.26 km a.g.l., reaching a maximum value of approximately 0.27 at around 18:00. Despite the influence of dust

https://doi.org/10.5194/egusphere-2026-2659
Preprint. Discussion started: 29 May 2026


events, a pronounced nose-shaped vertical distribution pattern was still observed. This indicates that elevated aerosol layers occurred more frequently and with greater intensity during the afternoon period. In contrast, the low frequency of elevated aerosol layers, coupled with the influence of dust events, resulted in the mean aerosol extinction coefficient profile at Minqin not exhibiting a distinct nose-shaped structure. Nevertheless, diurnal variation characteristics were still evident: the extinction coefficient was significantly higher from 10:00 to 18:00 than at night below 2 km a.g.l, particularly between 10:00 and 12:00, when the near-surface extinction coefficient exceeded 0.4, indicating a significant increase in aerosol loading within 2 km. The near-surface depolarisation ratio exhibited a similar trend, remaining mostly below 0.3 at both sites, with slightly higher values at Minqin. This earlier occurrence of the peak is mainly attributed to geographical differences between the two regions.

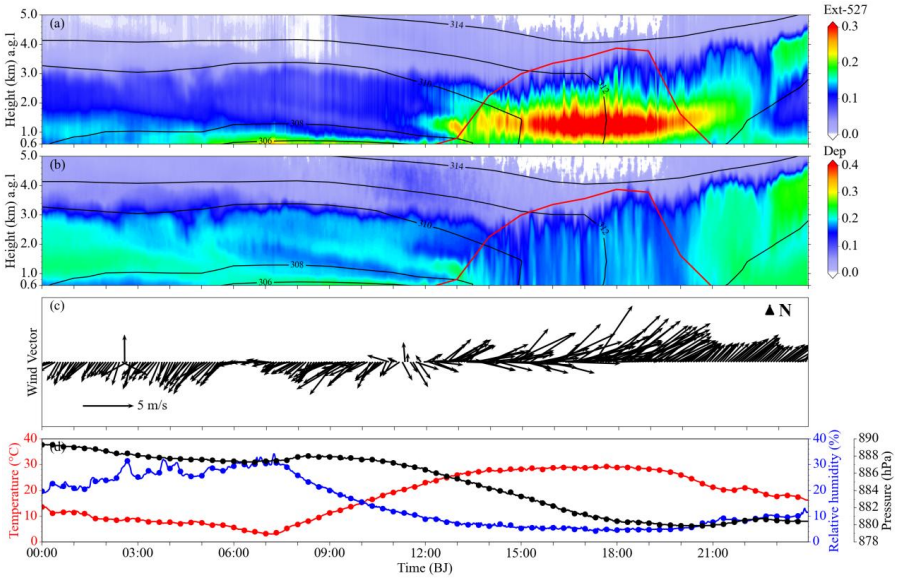


**Fig. 7. Time series of aerosol vertical distribution and meteorological parameters at Dunhuang on April 21 2012. (a) Time–height cross-sections of aerosol extinction coefficient and (b) depolarisation ratio derived from MPL lidar, with potential temperature contours (black lines) and boundary layer height (red lines) from ERA5. (c) wind vectors measured by an automatic meteorological station (model WXT520), and (d) temperature, relative humidity, pressure.**

Furthermore, two representative cases at both sites are presented to illustrate the diurnal variation of aerosol vertical distribution and the associated thermal and dynamical factors, particularly during periods when elevated aerosol layers occur. As shown in Fig. 7a–b, except during the period ( approximately 14:00–20:00 BJT) when the boundary layer is fully developed, the aerosol extinction coefficient at Dunhuang is relatively low (mean: 0.14 km-1), while the depolarization ratio remains

https://doi.org/10.5194/egusphere-2026-2659
Preprint. Discussion started: 29 May 2026


high (mean: 0.21), indicating low aerosol loading predominantly composed of polluted dust. When elevated aerosol layers were present from 15:00 to 20:00, a high aerosol extinction coefficient (~0.27 km-1) was observed at approximately 1 km, while the depolarisation ratio decreased to 0.17, indicating mixing with anthropogenic pollutants near the surface or with clearer air at the top of the boundary layer. During this period, AOD440nm ranged between 0.15 and 0.26, and AE440-870nm ranged between 0.3 and 0.5. Meanwhile, SSA exhibited a distinct wavelength dependence characteristic of dust- dominated aerosols (Dubovik et al., 2002; Tutsak and Koçak, 2020): values at 440 nm were consistently lower (0.86–0.88), whereas those at longer wavelengths (675, 870, and 1020 nm) were markedly higher (0.93–0.99) and increased with wavelength (not shown here). The potential temperature gradient weakened, indicating increased atmospheric stability. Within this layer, vertical motion was suppressed, and the atmosphere tended towards hydrostatic equilibrium, allowing aerosols to accumulate. As illustrated in Fig. 7c, the prevalence of southwesterly winds during elevated aerosol layer episodes suggests that aerosols originated from deserts located to the southwest. This is consistent with the backward trajectories of air masses presented in Fig. 1. In Fig. 7d, elevated aerosol layer episodes are accompanied by a rapid increase in surface temperature, reaching the daily maximum, while pressure and relative humidity decrease sharply. Comparisons with days without elevated aerosol layers show that the potential temperature profile varied gradually with time, and none of the aforementioned phenomena were observed (not shown here). This suggests that the formation of elevated aerosol layers is primarily driven by thermal processes.

https://doi.org/10.5194/egusphere-2026-2659
Preprint. Discussion started: 29 May 2026


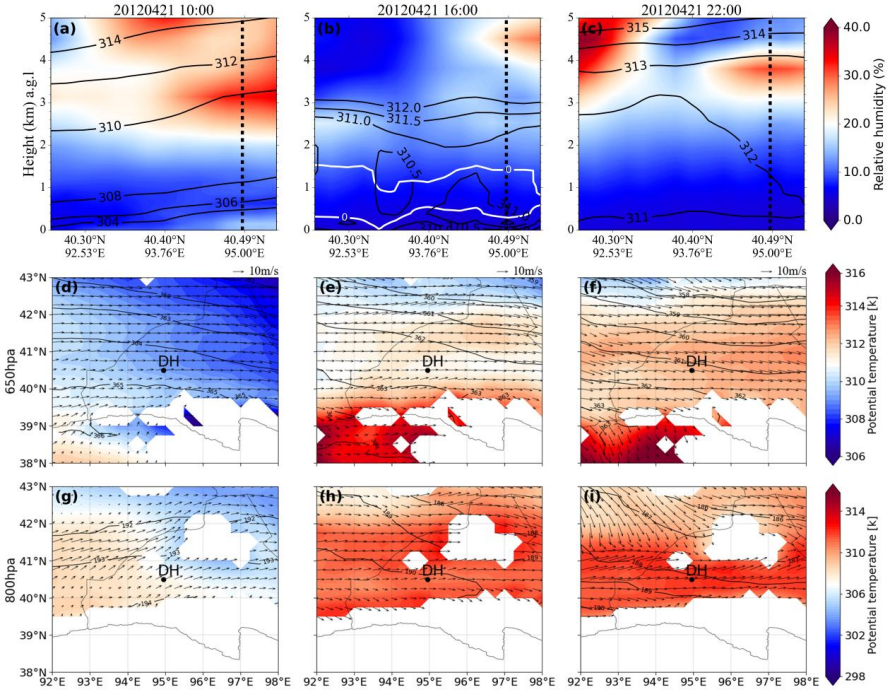


**Fig. 8. Thermal and dynamical fields at Dunhuang on 21 April 2012. (a–c) Vertical cross-sections of relative humidity with unstable stratification (demarcated by the white enclosed area) along the transect indicated by the red line in Fig. 1. Black solid lines represent isotherms, while black dashed lines denote the location of the observation site. (d–i) Meteorological fields at the 650 hPa and 800 hPa levels, with geopotential, height contours, during the experimental periods over the Dunhuang region. White regions indicate elevated mountain terrain.**

Along the HYSPLIT backward trajectories, a vertical cross-section of relative humidity and potential temperature reveal that the elevated transport and accumulation of aerosols over the Dunhuang region represent a typical thermodynamic coupling process with distinct diurnal variations. For the case shown in Fig. 8, three representative time points were selected to examine the evolution of the thermodynamic structure, representing the pre- (10:00), during (16:00) and post-event (22:00) stages of the elevated aerosol layer episode. During these three stages, near-surface relative humidity remained approximately 10% (Fig. 8a–c), consistent with observation shown in Fig. 7c. Such dry atmospheric conditions favour the development of strong surface thermal contrasts, which in turn drive the vertical uplift of aerosols (Mazza and Chen, 2025; Pal et al., 2025; Wen et al., 2025). To better characterise the elevated aerosol layer, the 650 hPa level is analysed (Fig. 8d–f), where westerly winds prevail persistently, with geopotential height exhibiting a consistent increase from north to south and a nearly constant gradient. No significant convective activity or prominent synoptic systems were

https://doi.org/10.5194/egusphere-2026-2659
Preprint. Discussion started: 29 May 2026


detected at this level. Only typical diurnal thermal variations of the air mass were observed. These characteristics indicate that atmospheric stratification at this level was highly stable. Under such meteorological conditions, stable stratification effectively suppresses vertical air motion and confines aerosols below this level (Haeffelin et al., 2024; Hu et al., 2024; Zhong et al., 2018a).

Before the elevated aerosol layer episodes, although the potential temperature at 800 hPa in the vicinity of the Dunhuang region remained relatively low, a thermal gradient had already developed between the desert areas to the west of the site and those to the east (Fig. 8g). In addition, the potential temperature gradient over the Dunhuang region was large, with gently sloping isentropic surfaces indicating stable stratification, which impeded the upward transport of aerosols and confined them to the near-surface layer (Zhu et al., 2011). As time progressed, intense daytime solar radiation strongly heated the surface in low-altitude areas, where low heat capacity allows rapid warming. This caused substantial increases in surface potential temperature, resulting in upward-bulging isentropic surfaces and a sharp decrease in the potential temperature gradient. Meanwhile, ascending airflows developed under the influence of thermal buoyancy (De Wekker et al., 2018), facilitating the upward transport of near-surface aerosols. During the formation of the elevated aerosol layer, the near-surface layer transitioned from stable to conditionally unstable, with unstable stratification observed at mean heights of approximately 0.3–1.3 km a.g.l (Fig. 8b), although the thickness of this layer varied considerably (Jin et al., 2022). Within this unstable stratification, the environmental lapse rate exceeded the dry adiabatic lapse rate. Consequently, rising air parcels cooled more slowly than the surrounding environment, maintaining positive buoyancy and accelerating upward —a key feature of absolute instability (Wang et al., 2022). Under such conditions, air parcels subjected to minor disturbances rose due to thermal buoyancy, facilitating the upward transport of near-surface aerosols. Upon reaching the overlying stable stratification, air parcels encountered negative buoyancy and tended towards hydrostatic equilibrium (Serafin et al., 2018), thereby inhibiting further vertical motion. As a result, aerosols accumulated within the altitude range of 0.6–2 km a.g.l and tended to concentrate near the base of the stable stratification. This finding is consistent with those reported in other regions (Su et al., 2020a; Meng et al., 2025). Following elevated aerosol layer episodes, surface cooling occurred as solar heating diminished. Despite the persistence of relatively high potential temperatures at this moment, isentropic surfaces gradually flattened and atmospheric stratification progressively returned to a stable state (Figure 8c). In combination with relatively strong wind speeds within this altitude layer (Fig. 8i),

https://doi.org/10.5194/egusphere-2026-2659
Preprint. Discussion started: 29 May 2026


these meteorological conditions facilitated the rapid dissipation of the elevated aerosol layer.

Furthermore, as illustrated in Fig. 8g–i, a distinct mountain–valley breeze circulation occurred near the Qilian Mountains throughout the development of the elevated aerosol layer, which may promote its diffusion and transport. This occurs because colder, denser air over the high terrain of the Qilian Mountains tends to flow downslope; however, as this air gradually warms after absorbing solar radiation, the downslope flow weakens. At the same altitude, the atmosphere over low-altitude areas warms less due to minimal absorption of shortwave radiation, whereas the air over high terrain is warmer and less dense, resulting in lower pressure compared with that at the same level over low-altitude areas. This pressure gradient drives airflow from low-altitude areas towards higher terrain, forming upslope winds (Cacciani et al., 2018; Serafin et al., 2018). Thus, daytime surface winds blow from low-altitude regions towards the Qilian Mountains, facilitating the transport of elevated aerosol layers towards the mountains (Fig. 8h), whereas the opposite occurs at night. However, in the case illustrated in Fig. 8, the prevailing wind direction was southwesterly during the formation of the elevated aerosol layer, and the Dunhuang site is located far from the Qilian Mountains. Consequently, the elevated aerosol layer exerted a negligible influence on the Qilian Mountains in this case. Nevertheless, as shown in Fig. 3, numerous cases characterised by prevailing northeasterly winds were recorded at the Dunhuang Site (not shown here). In these cases, elevated aerosol layers over the Dunhuang region would be strongly influenced by mountain-valley winds and transported towards the Qilian Mountains during the daytime. This process may contribute to localised pollution and may also accelerate snow and glacier melt (Hou et al., 2018).

https://doi.org/10.5194/egusphere-2026-2659
Preprint. Discussion started: 29 May 2026


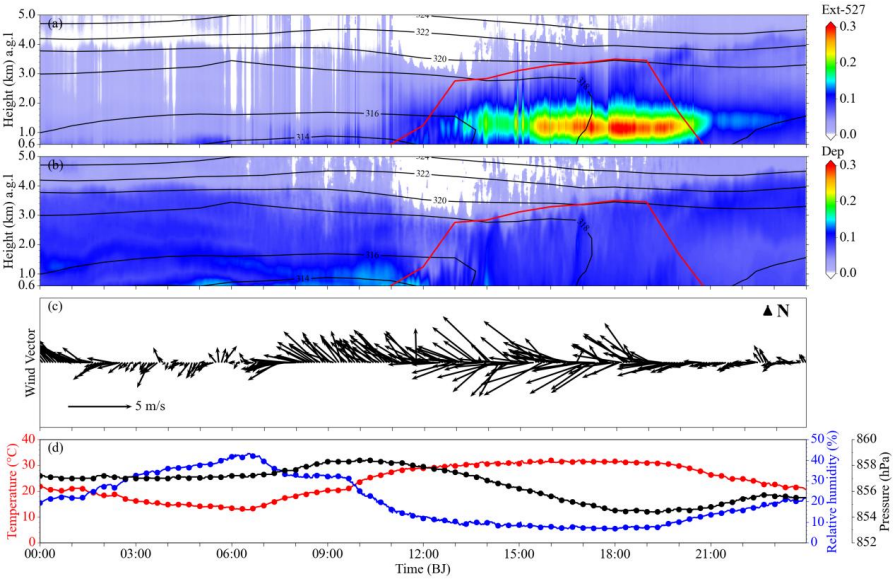


**Fig. 9. Same as Fig.7, but for the Minqin site on 14 June 2010.**

Similar to Fig. 7, a distinct elevated aerosol layer was observed at Minqin on 14 June 2010 (Fig. 9). Consistent with observation at Dunhuang, the average aerosol extinction coefficient at Minqin remained relatively low (~ 0.08 $km^{-1}$) for most of the observation period, except during the fully developed boundary layer stage (14:00–20:00 BJT), when it increased significantly to 0.23 $km^{-1}$. However, the depolarization ratio at Minqin showed minimal variation throughout the observation period and remained low, with a value of approximately 0.09. This indicates that the elevated aerosol layer was primarily composed of anthropogenic aerosols. Based on the optical properties, during the elevated aerosol layer episode, AOD440nm ranged from 0.08 to 0.14, and AE440-870nm ranged from 0.65 to 0.75. In parallel, SSA exhibited a distinct spectral signature characteristic of anthropogenic aerosols (Dubovik et al., 2002; Tutsak and Koçak, 2020): values at all four wavelengths (440, 675, 870, and 1020 nm) were comparable (0.86–0.92), with no pronounced gradient between short and long wavelengths (not shown here). Collectively, these parameters indicate that the elevated aerosol layer exhibited lower aerosol loading, a higher fraction of fine-mode particles, and stronger scattering capability (Budhavant et al., 2020; Jangid et al., 2024). Similar to Fig. 7, the case presented here represents only one example and does not imply that elevated aerosol layers at both sites are dominated by a single type of mixed aerosol. Combined with Fig. 4–5, it can be observed that both scenarios occurred at both sites during the experimental periods, with differences likely arising from variations in

https://doi.org/10.5194/egusphere-2026-2659
Preprint. Discussion started: 29 May 2026


dust aerosol content. Although not exclusively dominated by a single type, certain aerosol types exhibit higher occurrence frequencies and greater representativeness in each region. Additionally, consistent with observations at Dunhuang, the weakening potential temperature gradient implies that the atmosphere was stably stratified. As shown in Fig. 9c, easterly winds prevailed during the aerosol layer episode. This transport pathway is consistent with the backward trajectories of air masses presented in Fig. 1. A similar pattern of the diurnal variations in temperature, humidity, and pressure is observed in Fig. 9d, indicating that thermal processes are also the primary drivers of the elevated aerosol layer.

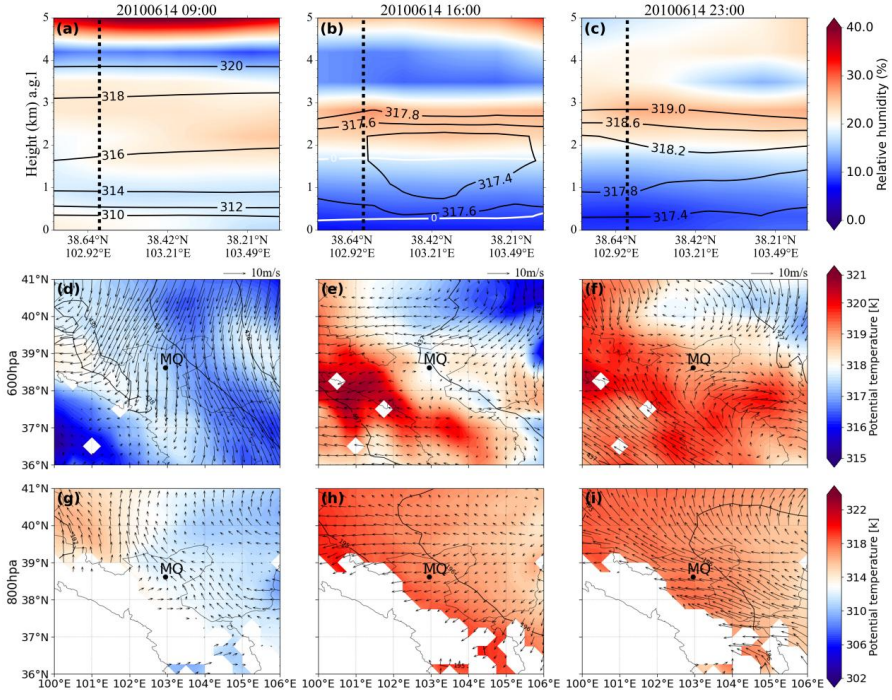


**Fig. 10. Same as Fig. 8, but for Minqin on 14 June 2010. The meteorological conditions correspond to the 600 and 800 hPa levels.**

Consistent with the approach adopted for Fig. 7, three time points were selected to represent the evolution of the thermodynamic structure, corresponding to the pre- (09:00), during (16:00) and post-event (23:00) stages of the elevated aerosol layer episode in Fig. 10. This selection of time points is based on earlier initiation and later dissipation of the elevated aerosol layer in the Fig. 9 case compared with that in Fig. 7. A similar formation and transport mechanism of elevated aerosol layers is also observed at Minqin, representing a typical thermodynamic coupling process with pronounced diurnal variations. Elevated aerosol layers form under thermal forcing and are subsequently transported

https://doi.org/10.5194/egusphere-2026-2659
Preprint. Discussion started: 29 May 2026


towards the Qilian Mountains region, driven by mountain–valley wind circulation.

In contrast to Dunhuang, a pronounced abrupt change in relative humidity occurs at the upper boundary of the unstable stratification, with a larger vertical extent and nearly constant height, where a persistent high-relative-humidity zone is present (Fig.10a–c). This indicates a strong correlation between relative humidity and the vertical extent of the unstable stratification, further suggesting that the accumulation of water vapor exerts a significant inhibitory effect on the upward transport of near-surface aerosols (Zhong et al., 2018b; Wang et al., 2020). Analysis of the corresponding height layer at the 600 hPa level (Fig. 10d–f) shows that, before the elevated aerosol layer episodes, potential temperature was relatively low, with cold air masses dominating. The wind direction was predominantly northerly, and geopotential height increased from northeast to southwest. A cyclone was located to the southwest of the region, where subsiding airflows prevailed and conditions were relatively clear. However, this cyclone was located at some distance from the Minqin site; no significant large-scale synoptic systems or convective activity were present in its vicinity. This indicates that atmospheric stratification at this level was stable, confining aerosols below this layer. During elevated aerosol layer episodes, the site was situated near the boundary between cold and warm fronts (Fig.10e). This frontal zone led to enhanced relative humidity at this level (Zhang et al., 2007). During this process, warm, moist air ascended over the colder air mass, forming a frontal inversion that suppressed vertical motion and inhibited atmospheric mixing (Feng et al., 2023). Following the elevated aerosol layer episodes, warm air masses dominated over the site, with an anticyclone to the southeast associated with ascending airflows and a cold frontal shear line to the north. These synoptic conditions favour an increase in water vapor content (Peng, 2013). Additionally, mountain–valley wind effect circulation is markedly more intense (Fig. 10g–i).

https://doi.org/10.5194/egusphere-2026-2659
Preprint. Discussion started: 29 May 2026


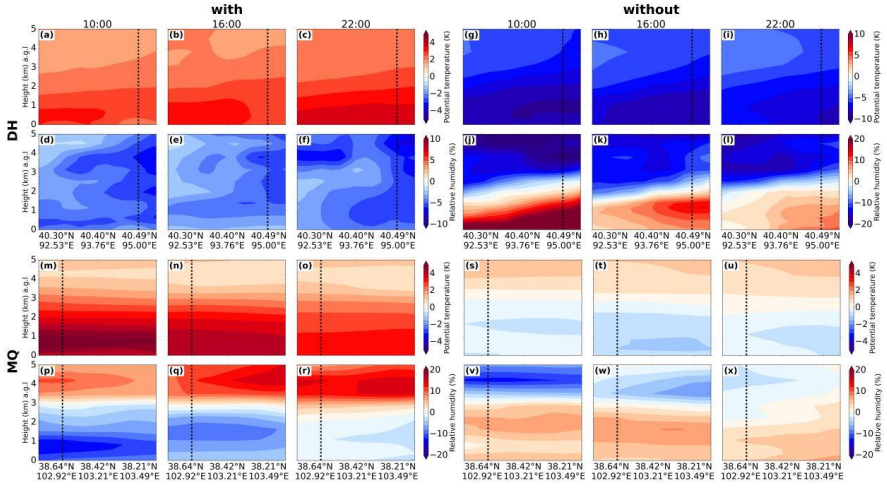


**Fig.11. Anomalies of potential temperature and relative humidity between the mean states during periods with and without elevated aerosol layers and the summer climatological state at Dunhuang and Minqin.**

As shown in Fig. 11, during cases when elevated aerosol layer occurred at Dunhuang and Minqin, the potential temperature below 3 km at both sites exhibited a positive anomaly of 3–5 K (Fig. 11a–c, m–o), significantly deviating from the average boundary layer potential temperature (~310 K) at the two sites during the experiment period. Meanwhile, relative humidity below this altitude was generally 5–10% lower than the average value (~30%) (Fig. 11d–f, p–r), indicating distinctly warm and dry anomalous meteorological conditions in the lower atmosphere. Notably, during cases at Minqin, positive relative humidity anomalies of 5–15% appeared above approximately 3 km, consistent with those shown in Fig. 10a–c. This suggests that the region may be frequently influenced by the convergence of cold and warm air masses. This vertical humidity distribution is consistent with previous findings that high-humidity conditions near the top of the boundary layer favour the retention and accumulation of aerosols within the boundary layer (Harm-Altstädter, 2018). In contrast, when elevated aerosol layers did not occur, the potential temperature at both sites showed a negative anomaly of 1–6 K (Fig. 11g–i, s–u), and relative humidity was 5–25% higher than the average state (Fig. 11j–l, v–x). Based on these observations, there is a significant correlation between boundary layer temperature and humidity anomalies and the occurrence of elevated aerosol layers. Most elevated aerosol layer events occur under the PN state characterised by positive potential temperature anomalies and negative relative humidity anomalies. Under the PN state, intense solar radiation (high potential temperature) and a dry surface (low humidity) result in weak evaporative cooling. Consequently, most

https://doi.org/10.5194/egusphere-2026-2659
Preprint. Discussion started: 29 May 2026


net radiation is converted into sensible heat, leading to strong heating of near-surface air. This process favours the development of strong surface thermal contrasts and local thermal circulations, which facilitate the uplift of near-surface aerosols. However, the resulting low-humidity air parcels are characterised by a high lifting condensation level (Lal et al., 2023). This increases the difficulty of convection initiation, inhibits the enhancement of convective development by latent heat release, and favours the uplift, accumulation and persistence of aerosols, thereby promoting the formation of elevated aerosol layers. Based on these findings, a simplified conceptual prediction model for elevated aerosol layers can be constructed, with key early-warning indicators being positive anomalies in boundary layer potential temperature and negative anomalies in boundary layer relative humidity. When both indicators are satisfied simultaneously, this can be identified as a high-probability early-warning period for the occurrence of elevated aerosol layers.

### 3.3 Air quality and radiative effects

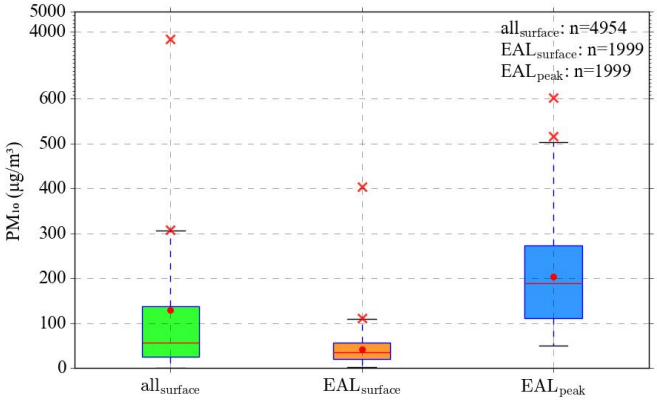


**Fig.12. Boxplots of PM10 concentrations during the experiment at the Dunhuang site, including surface values for all days, surface values during elevated aerosol layer (EAL) days, and peak values within elevated aerosol layers. The red lines represent the median, red dots indicate the mean values, the box edges denote the 25th and 75th percentiles (Q1 and Q3), and the whiskers represent non-outlier data points. Outliers (values beyond Q3 + 1.5 × IQR or below Q1 − 1.5 × IQR) are marked with red crosses, with only the minimum and maximum outliers labelled for clarity. Under a normal distribution, the whiskers encompass approximately 99% of the data.**

During both experimental periods, PM10 mass concentration observations were available only at Dunhuang. Here, the conversion method described in Section 2 was used to assess the air pollution levels of elevated aerosol layers. As shown in Fig. 12, PM10 concentration at the near-surface and at the peak of elevated aerosol layers are presented. The average near-surface PM10 concentration across all observations was 129.6 ± 212.0 μg/m³ during the entire experimental period. During elevated

https://doi.org/10.5194/egusphere-2026-2659
Preprint. Discussion started: 29 May 2026


aerosol layer episodes, the near-surface average PM10 concentration decreased to 40.8 ± 30.4 μg/m³, whereas the average concentration at the peak of the elevated aerosol layers reached 203.3 ± 106.6 μg/m³. The peak concentration is nearly five times higher than that at the near-surface. This concentration approaches levels observed during severe haze events. For instance, previous studies reported that a severe haze event in Beijing, China recorded an average PM10 concentration of 265.2 ± 157.1 μg/m³ (Wang et al., 2015). PM10 concentrations during haze and dust events in South Korea reached 163.9 ± 25.0 μg/m³ and 211.3 ± 57.5 μg/m³, respectively (Jung et al., 2017; Seo et al., 2017). This clearly indicates that even when surface pollution is low or negligible, a highly concentrated pollutant aerosol layer may exist in the upper boundary layer. Although PM10 concentration observations are only available from Dunhuang, the periods of elevated aerosol layer occurrence during daytime and their associated thermodynamic conditions are similar at both sites, as shown in Figs. 7, 9 and 11. Therefore, it can be inferred that such elevated aerosol layers may occur throughout the Hexi Corridor region under similar meteorological conditions, exerting a significant impact on the regional environment. These findings highlight that, when assessing air quality and developing pollution control strategies, reliance solely on surface-level monitoring is insufficient. Instead, elevated aerosol layers within the boundary layer should be comprehensively considered, as their formation and dispersion are closely related to surface pollutant level (Dong et al., 2022).

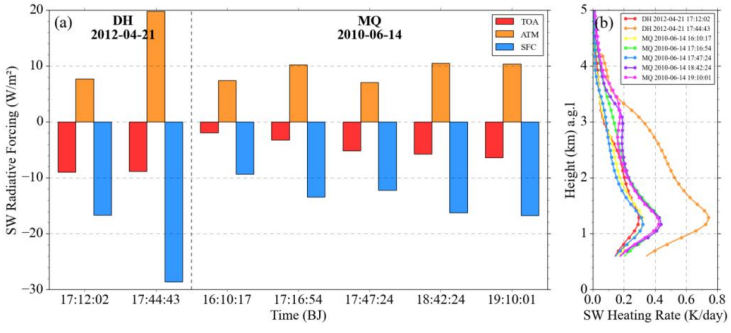


**Fig. 13. Radiative effects of elevated aerosol layers. (a) Histograms of aerosol shortwave radiative forcing (SWRF) at Dunhuang and Minqin, with red, orange, and blue bars representing the surface (SFC), atmosphere (ATM), and top of the atmosphere (TOA), respectively; (b) vertical profiles of shortwave heating rate at Dunhuang and Minqin.**

The presence of elevated aerosol layers not only increases air pollution levels over the Hexi Corridor region but also exerts significant regional radiative effects. Simulated shortwave radiative forcing results for two elevated aerosol layer events—observed on 21 April 2012 at Dunhuang and on

https://doi.org/10.5194/egusphere-2026-2659
Preprint. Discussion started: 29 May 2026


14 June 2010 at Minqin—are presented (Fig. 13a). At the surface (SFC), the average shortwave radiative forcing at Dunhuang was −22.66 W/m², with a significantly larger magnitude than that at Minqin (−13.60 W/m²). This indicates a stronger surface cooling effect induced by elevated aerosol layers at Dunhuang. In addition, these effects reduce solar radiation reaching the surface during daytime and can directly affect the efficiency of photovoltaic power generation. This value exceeds the shortwave radiative forcing at the SFC reported for a moderate dust event (−19.5 W/m²) (Li et al., 2025) and is comparable to the −23 W/m² observed during dust events (Marsli et al., 2025). The value at Minqin is stronger than that for a light dust event (−12.0 W/m²) reported by (Li et al., 2025), and is comparable to mineral dust events (−13.65 W/m²) reported by (Barragan et al., 2020). Radiative forcing at the top of atmosphere (TOA) was negative at both sites, averaging −8.92 W/m² at Dunhuang, with a larger magnitude than −4.49 W/m²at Minqin, which is close to the −4 W/m² reported for dust events (Marsli et al., 2025). This value is comparable to a mineral dust event (−9.1 W/m²) observed over the Iberian Peninsula (Barragan et al., 2020) but significantly higher than −2.7 W/m² and −4.0 W/m²during two other dust events at Dunhuang recorded by (Bi et al., 2014). These findings demonstrate that elevated aerosol layers exert a cooling effect in both regions. Elevated aerosol layers at Dunhuang exert a more pronounced effect on increasing the planetary albedo, thereby producing a stronger suppression of the surface radiation budget. Additionally, the average atmospheric (ATM) shortwave radiative forcing at Dunhuang is 13.74 W/m², higher than 9.10 W/m² at Minqin. This suggests that elevated aerosol layers at Dunhuang are more efficient at intercepting and redistributing solar radiation, with atmospheric radiative forcing higher than 5.1 W/m² reported for a dust event (Bran et al., 2018), but lower than 16.94 W/m² reported for a mineral dust event over the Iberian Peninsula (Barragan et al., 2020). Atmospheric (ATM) shortwave radiative forcing reflects the energy absorbed by aerosols and converted into heat within the atmosphere. The peak shortwave heating rate (Jangid et al., 2024) reached 0.74 K/day at Dunhuang and 0.44 K/day at Minqin, with the value at Dunhuang comparable to the peak heating rate (~0.7 K/day) reported for a light dust event (Li et al., 2025). The mean shortwave heating rates (SHR) at both sites (0.23 K/day at Dunhuang and 0.14 K/day at Minqin) were higher than those observed during several dust events at Dunhuang (Bi et al., 2014) (e.g., 0.1 K/day and 0.14 K/day on 9 and 10 April 2012, respectively), as well as those recorded over Issyk-Kul Lake (0.08 K/day) (Gan et al., 2025) and southern Portugal (0.11 K/day) (Valenzuela et al., 2016). This indicates that elevated aerosol layers absorb solar shortwave radiation, leading to significant

https://doi.org/10.5194/egusphere-2026-2659
Preprint. Discussion started: 29 May 2026


atmospheric heating. This may influence regional weather processes and climate feedback mechanisms by altering the local thermal structure and vertical stability (Huang et al., 2009).

Considering snow cover conditions in the Qilian Mountains, seasonal snow is primarily distributed at altitudes of 3–4 km (equivalent to 1.5–2.5 km a.g.l.) (Guo et al., 2021), which coincides with the altitude range of elevated aerosol layers. After deposition in the Qilian Mountains, these pollutants significantly reduce snow albedo, enabling the surface to absorb more solar radiation. Simultaneously, as indicated by the SHR of the elevated aerosol layer, the layer itself maintains a relatively high temperature due to its absorption of shortwave radiation, and the resulting heat further accelerates snowmelt. This combined effect accelerates snowmelt and glacier retreat. Therefore, radiative forcing associated with elevated aerosol layer can induce regional warming in the Qilian Mountains, similar to the warming effect of brown clouds over the Indian Peninsula, which accelerates snowmelt in the Himalayas (Ramanathan et al., 2007). This is of considerable concern, as it is directly linked to regional water security and storage. In addition, the Hexi Corridor is also an important solar energy base, the elevated aerosol layer weakens the solar radiation reaching the surface during daytime, thereby directly affecting photovoltaic power generation efficiency (Wang et al., 2026).

## 4. Conclusion

Based on intensive observation campaigns in 2010 and 2012 over the Hexi Corridor in Northwest China, this study first reveals the occurrence of elevated aerosol layers within the daytime mixed layer in this region and further examines their vertical distribution characteristics, formation mechanisms from a diurnal perspective, and environmental and radiative effects. The results show that distinct elevated aerosol layers occur at approximately 0.6–2 km during daytime at both Dunhuang and Minqin. Excluding dust events, the occurrence frequencies of elevated aerosol layers are approximately 81% and 37% at Dunhuang and Minqin, respectively, with peak occurrence concentrated in May and June. Aerosols at Dunhuang are characterised as dust-dominated mixtures, whereas those at Minqin are dominated by anthropogenic pollutants, with each dominant type occurring more frequently in its respective region. The formation of elevated aerosol layers is controlled by a coupled thermodynamic process: surface heating causes the boundary layer to transition from stable to conditionally unstable during daytime, facilitating the upward transport and accumulation of aerosols at the base of the stable

https://doi.org/10.5194/egusphere-2026-2659
Preprint. Discussion started: 29 May 2026


layer, which are subsequently transported towards the adjacent Qilian Mountains by mountain–valley winds. Additionally, conditions at Minqin are influenced by frontal inversions and water vapour. Thus, a simplified conceptual model for the prediction of elevated aerosol layer occurrence is proposed, based on positive anomalies in potential temperature and negative anomalies in relative humidity within the boundary layer. Regarding environmental impacts, the peak PM10 concentration within the elevated aerosol layer (203.3 ± 106.6 μg/m³) is approximately five times higher than that at the surface (40.8 ± 30.4 μg/m³), indicating that reliance solely on surface observations would substantially underestimate the regional pollution burden. Meanwhile, such layers enhance the atmospheric shortwave heating rate by up to 0.7 K/day, a magnitude comparable to that associated with light dust loading. Notably, the mean shortwave heating rates at both sites are higher than those reported during several dust events at Dunhuang. Furthermore, elevated aerosol layers are likely to accelerate glacier retreat and snow melt by reducing snow/ice albedo and enhancing radiative absorption, thereby posing a potential threat to regional water resource security, particularly under the influence of mountain–valley winds.

This study provides crucial observational evidence for the existence of elevated aerosol layers in the Hexi Corridor region, highlighting their significant scientific importance for regional air pollution prevention and control, ecosystem protection in complex terrains, and water resource security in ecologically sensitive areas of northwest China. However, the limited observations remain insufficient for a comprehensive understanding of the formation, maintenance, long-term evolution, and regional impacts of elevated aerosol layers. Additional field observations and model simulations across other parts of the Hexi Corridor and the adjacent Qilian Mountains are needed to further investigate their impacts.

https://doi.org/10.5194/egusphere-2026-2659
Preprint. Discussion started: 29 May 2026


**CRediT authorship contribution statement**

Zikai Lin: Writing – original draft, Software, Resources, Methodology, Investigation, Formal analysis, Data curation. Tian Zhou: Writing – review & editing, Writing – original draft, Supervision, Project administration, Funding acquisition, Data curation, Conceptualization. ZhengPeng Li: Software, Resources, Methodology, Investigation, Formal analysis, Data curation. Yonghong Gu: Software, Resources, Methodology, Investigation, Formal analysis. Dongsheng Wu: Software, Resources, Methodology, Investigation, Formal analysis. Ping Zhou: Methodology, Resources, Software, Data curation. Keyu Zhang: Software, Resources, Methodology, Data curation. Qili Gao: Software, Resources, Methodology, Data curation. Xingran Li: Software, Resources, Methodology, Data curation. Zhongwei Huang: Writing – review & editing, Validation, Supervision, Project administration, Data curation, Conceptualization. Jianrong Bi: Writing – review & editing, Writing – original draft, Supervision, Project administration, Data curation, Conceptualization. Lili Yang: Writing – review & editing, Writing – original draft, Supervision, Project administration, Data curation, Conceptualization. Lina Wang: Writing – review & editing, Writing – original draft, Supervision, Project administration, Data curation, Conceptualization.

**Competing interests**

The contact author has declared that none of the authors has any competing interests.

**Data availability**

The ERA-5 reanalysis data are available from the ECMWF at https://cds.climate.copernicus.eu/datasets/reanalysis-era5-single-levels?tab=overview. The AERONET data are provided by the NASA and can be accessed at https://aeronet.gsfc.nasa.gov. The HYSPLIT data is sourced from the NOAA and can be accessed at https://www.arl.noaa.gov/hysplit/. SBDART model can be downloaded and installed from https://github.com/paulricchiazzi/SBDART.

**Financial support**

This research was funded by Fundamental and Interdisciplinary Disciplines Breakthrough Plan of the Ministry of Education of China (JYB2025XDXM910), the National Science Foundation of China

https://doi.org/10.5194/egusphere-2026-2659
Preprint. Discussion started: 29 May 2026


(42475078), the Gansu Science and Technology Major Program (24ZDWA006), the Gansu Provincial Science and Technology Program (23JRRA1032), and the China '111' Project (B25040).

**Acknowledgements**

The authors would like to express their sincere thanks to all personnel involved in the intensive field observations. We are grateful to the ERA5 team for providing the reanalysis data used in this study. We appreciate the Earth Space Research Group, Institute for Computational Earth System Science, University of California, Santa Barbara, for their contribution to the SBDART model used in this study. We also thank the anonymous reviewers for their insightful and valuable comments.

**References**

Albergel, C., Dutra, E., Munier, S., Calvet, J.-C., Munoz-Sabater, J., de Rosnay, P., Balsamo, G. J. H., and Sciences, E. S.: ERA-5 and ERA-Interim driven ISBA land surface model simulations: which one performs better?, Hydrology and Earth System Sciences, 22, 3515-3532, 2018.

Barragan, R., Molero, F., Granados-Muñoz, M., Salvador, P., Artíñano, B., and Pujadas, M.: Feasibility of Ceilometers Data to Estimate Radiative Forcing Values: Application to Different Conditions around the COVID-19 Lockdown Period, Remote Sensing, 10.3390/rs12223699, 2020.

Bi, J., Shi, J., Xie, Y., Liu, Y., Takamura, T., and Khatri, P.: Dust Aerosol Characteristics and Shortwave Radiative Impact at a Gobi Desert of Northwest China during the Spring of 2012, Journal of the Meteorological Society of Japan. Ser. II, 92A, 33-56, 10.2151/jmsj.2014-A03, 2014.

Bi, J., Huang, J., Shi, J., Hu, Z., Zhou, T., Zhang, G., Huang, Z., Wang, X., and Jin, H.: Measurement of scattering and absorption properties of dust aerosol in a Gobi farmland region of northwestern China – a potential anthropogenic influence, Atmos. Chem. Phys., 17, 7775-7792, 10.5194/acp-17-7775-2017, 2017.

Boselli, A., Wang, X. A., Armenante, M., D'Avino, L., Pisani, G., and Spinelli, N.: Study of a multy-layered structure of aerosol vertical distribution over Naples performed during earlinet project, 22ND INTERNATIONAL LASER RADAR CONFERENCE (ILRC 2004), VOLS 1 AND 2, WOS:000223133500219200 4.

Boselli, A., Armenante, M., D'Avino, L., D'Isidoro, M., Pisani, G., Spinelli, N., and Wang, X.: Atmospheric Aerosol Characterization Over Naples During 2000-2003 EARLINET Project: Planetary Boundary-Layer Evolution and Layering, BOUNDARY-LAYER METEOROLOGY, 132, 151-165, 10.1007/s10546-009-9382-6, 2009.

Bran, S., Jose, S., and Srivastava, R.: Investigation of optical and radiative properties of aerosols during an intense dust storm: A regional climate modeling approach, Journal of Atmospheric and Solar-Terrestrial Physics, 168, 10.1016/j.jastp.2018.01.003, 2018.

Budhavant, K. B., Gawhane, R. D., Rao, P. S. P., Nair, H. R. C. R., and Safai, P. D.: Physico-chemical characterization and sink mechanism of atmospheric aerosols over South-west India, Journal of Atmospheric Chemistry, 77, 17-33, 10.1007/s10874-020-09400-x, 2020.

https://doi.org/10.5194/egusphere-2026-2659
Preprint. Discussion started: 29 May 2026


Cacciani, M., Kossmann, M., Knievel, J. C., Giovannini, L., Gutmann, E. D., and Zardi, D.: Meteorological Applications Benefiting from an Improved Understanding of Atmospheric Exchange Processes over Mountains, Atmosphere, 9, 371, 10.3390/atmos9100371, 2018.

Che, H., Xia, X., Zhao, H., Li, L., Gui, K., Zheng, Y., Song, J., Qi, B., Zhu, J., Miao, Y., Wang, Y., Wang, Z., Wang, H., Dubovik, O., Holben, B., Chen, H., Shi, G., and Zhang, X.: Aerosol optical and radiative properties and their environmental effects in China: A review, Earth-Science Reviews, 248, 10.1016/j.earscirev.2023.104634, 2024.

Chen, Q., Yin, Y., Jin, L.-j., Xiao, H., and Zhu, S.-c.: The effect of aerosol layers on convective cloud microphysics and precipitation, Atmospheric Research, 101, 327-340, 10.1016/j.atmosres.2011.03.007, 2011.

Cheng, Y. M., Dai, T., Li, J. M., and Shi, G. Y.: Measurement Report: Determination of aerosol vertical features on different timescales over East Asia based on CATS aerosol products, ATMOSPHERIC CHEMISTRY AND PHYSICS, 20, 15307-15322, 10.5194/acp-20-15307-2020, 2020.

Dang, J., Xie, X., and Wen, X.: Evaluation of Boundary Layer Characteristics at Mount Si'e Based on UAV and Lidar Data, Remote Sensing, 16, 3816, 10.3390/rs16203816, 2024.

De Wekker, S. F. J., Kossmann, M., Knievel, J. C., Giovannini, L., Gutmann, E. D., and Zardi, D.: Meteorological Applications Benefiting from an Improved Understanding of Atmospheric Exchange Processes over Mountains, Atmosphere, 9, 371, 10.3390/atmos9100371, 2018.

DeRepentigny, P.: When fire and ice meet, Nature Climate Change, 14, 1224-1225, 10.1038/s41558-024-02183-z, 2024.

Diya, Kuppili, S. K., and Nagendra, S. M. S.: Air quality in different urban hotspots in a metropolitan city in India and the environmental implication, Environmental Monitoring and Assessment, 196, 10.1007/s10661-024-13272-z, 2024.

Dong, Q., Huang, Z., Li, W., Li, Z., Song, X., Liu, W., Wang, T., Jianrong, B., and Shi, J.: Polarization Lidar Measurements of Dust Optical Properties at the Junction of the Taklimakan Desert–Tibetan Plateau, Remote Sensing, 14, 558, 10.3390/rs14030558, 2022.

Du, Q., Zhao, C., Zhang, M., Dong, X., Chen, Y., Liu, Z., Hu, Z., Zhang, Q., Li, Y., Yuan, R., and Miao, S.: Modeling diurnal variation of surface PM <sub>2.5</sub> concentrations over East China with WRF-Chem: impacts from boundary-layer mixing and anthropogenic emission, Atmospheric Chemistry and Physics, 20, 2839-2863, 10.5194/acp-20-2839-2020, 2020.

Dubovik, O., Holben, B., Eck, T. F., Smirnov, A., Kaufman, Y. J., King, M. D., Tanré, D., and Slutsker, I.: Variability of Absorption and Optical Properties of Key Aerosol Types Observed in Worldwide Locations, Journal of the Atmospheric Sciences, 59, 590-608, https://doi.org/10.1175/1520-0469(2002)059<0590:VOAAOP>2.0.CO;2, 2002.

Feng, X., Zhang, Z., Guo, J., and Wang, S.: Multilayer inversion formation and evolution during persistent heavy air pollution events in the Sichuan Basin, China, Atmospheric Research, 286, 106691, 10.1016/j.atmosres.2023.106691, 2023.

Fountoulakis, I., Papachristopoulou, K., Proestakis, E., Amiridis, V., Kontoes, C., and Kazadzis, S.: Effect of Aerosol Vertical Distribution on the Modeling of Solar Radiation, Remote Sensing, 14, 1143, 10.3390/rs14051143, 2022.

Gan, Y., Zhang, Z., Chu, W., Ding, J., and Ren, Y.: Assessment and prediction of dust emissions, deposition and radiation forcing in Central Asia, 10.5194/egusphere-2025-965, 2025.

https://doi.org/10.5194/egusphere-2026-2659
Preprint. Discussion started: 29 May 2026


Guo, J., Yin, Y., Xu, M., Wu, J., Liu, D., Fan, W., and Lu, P.: Numerical study of aerosol radiative forcing over East Asia and the impacts of cloud coverage and relative humidity, Atmospheric Research, 273, 106168, https://doi.org/10.1016/j.atmosres.2022.106168, 2022.

Guo, Z., Wang, N., Shen, B., Gu, Z., Wu, Y., and Chen, A.: Recent Spatiotemporal Trends in Glacier Snowline Altitude at the End of the Melt Season in the Qilian Mountains, China, Remote Sensing, 13, 4935, 10.3390/rs13234935, 2021.

Haeffelin, M., Ribaud, J. F., Céspedes, J., Dupont, J. C., Lemonsu, A., Masson, V., Nagel, T., and Kotthaus, S.: Impact of boundary layer stability on urban park cooling effect intensity, Atmos. Chem. Phys., 24, 14101-14122, 10.5194/acp-24-14101-2024, 2024.

Hara, K., Takashima, H., Yoshino, A., Takami, A., Nishita-Hara, C., Fujiyoshi, Y., and Hayashi, M.: Seasonal variations of diurnal cycles of aerosols and gases in the Fukuoka Plain, Japan: Effects of local meteorology and atmospheric chemistry, Atmospheric Environment, 289, 10.1016/j.atmosenv.2022.119318, 2022.

Harm-Altstädter, B.: Airborne observations of newly formed boundary layer aerosol particles under cloudy conditions, Atmospheric Chemistry and Physics, 2018.

Holben, B. N., Eck, T. F., Slutsker, I., Tanré, D., Buis, J. P., Setzer, A., Vermote, E., Reagan, J. A., Kaufman, Y. J., Nakajima, T., Lavenu, F., Jankowiak, I., and Smirnov, A.: AERONET—A Federated Instrument Network and Data Archive for Aerosol Characterization, Remote Sensing of Environment, 66, 1-16, https://doi.org/10.1016/S0034-4257(98)00031-5, 1998.

Hou, X., Fei, D., Kang, H., Zhang, Y., and Gao, J.: Seasonal statistical analysis of the impact of meteorological factors on fine particle pollution in China in 2013–2017, Natural Hazards, 93, 677-698, 10.1007/s11069-018-3315-y, 2018.

Hu, Y., Yu, H., Kang, S., Yang, J., Rai, M., Yin, X., Chen, X., and Chen, P.: Aerosol–meteorology feedback diminishes the transboundary transport of black carbon into the Tibetan Plateau, Atmos. Chem. Phys., 24, 85-107, 10.5194/acp-24-85-2024, 2024.

Huang, J., Wang, T., Wencai, W., Li, Z., and Yan, H.: Climate effects of dust aerosols over East Asian arid and semiarid regions, Journal of Geophysical Research Atmospheres, 119, 10.1002/2014JD021796, 2014.

Huang, J., Q, F., J, S., Q, T., Hu, Y., Yi, H., and Zhao, Q.: Taklimakan dust aerosol radiative heating derived from CALIPSO observations using the Fu-Liou radiation model with CERES constraints, Atmospheric Chemistry and Physics, 9, 10.5194/acp-9-4011-2009, 2009.

Huang, Z., Dong, Q., Zhou, T., Jianrong, B., Chen, R., Qiantao, L., Abdullaev, S., Nozirov, D., Alam, K., Wang, T., Li, W., Li, Z., Song, X., and Liu, W.: Vertical distribution, optical properties, and source attribution of summer dust in southern Tajikistan: ground-based observations and model results, Atmospheric Environment, 361, 121514, 10.1016/j.atmosenv.2025.121514, 2025.

Huang, Z., Huang, J., Jianrong, B., Wang, T., Zhou, T., Dong, Q., Shi, J., Qiantao, L., Li, W., Li, Z., Song, X., Liu, W., Wang, H., and Niu, Z.: Dust observation by a ground-based lidar network along the global dust belt, E3S Web of Conferences, 575, 02006, 10.1051/e3sconf/202457502006, 2024.

Huige, D., Siwen, L., Yun, Y., Dengxin, H., and jianyu, W.: Observational study of the vertical aerosol and meteorological factor distributions with respect to particulate pollution in Xi'an, Atmospheric Environment, 247, 118215, https://doi.org/10.1016/j.atmosenv.2021.118215, 2021.

Huszar, P., Karlický, J., Ďoubalová, J., Šindelářová, K., Nováková, T., Belda, M., Halenka, T., Žák, M., and Pišoft, P.: Urban canopy meteorological forcing and its impact on ozone and PM2.5: role of vertical turbulent transport, Atmos. Chem. Phys., 20, 1977-2016, 10.5194/acp-20-1977-2020, 2020.

https://doi.org/10.5194/egusphere-2026-2659
Preprint. Discussion started: 29 May 2026


Jangid, M., Sankhla, T. S., Singh, S., and Mishra, A. K.: Radiative effect of atmospheric Brown clouds over the Indo-Gangetic plain, Atmospheric Pollution Research, 15, 102085, 10.1016/j.apr.2024.102085, 2024.

Jia, S., Sarkar, S., Zhang, Q., Wang, X., Wu, L., Chen, W., Huang, M., Zhou, S., Zhang, J., Yuan, L., and Yang, L.: Characterization of diurnal variations of PM2.5 acidity using an open thermodynamic system: A case study of Guangzhou, China, Chemosphere, 202, 677-685, 10.1016/j.chemosphere.2018.03.127, 2018.

Jian, B., Ma, Z., Liu, Q., Li, Z., Deng, L., Nie, H., Liu, C., Zhao, C., Sun, J., and Shen, X.: An advanced double-moment cloud microphysics scheme with explicit aerosol-cloud interactions and its performance in quantitative precipitation forecasting (QPF) in the CMA-MESO V5.0, Atmospheric Research, 108649, 10.1016/j.atmosres.2025.108649, 2025.

Jin, H.-G., Baik, J.-J., Lee, H., and Ahmed, T.: A new warm-cloud collection and breakup parameterization scheme for weather and climate models, Atmospheric Research, 272, 106145, 10.1016/j.atmosres.2022.106145, 2022.

Jung, J., Yu, J., Lyu, Y., Lee, M., Hwang, T., and Lee, S.: Ground-based characterization of aerosol spectral optical properties of haze and Asian dust episodes under Asian continental outflow during winter 2014, Atmos. Chem. Phys., 17, 5297-5309, 10.5194/acp-17-5297-2017, 2017.

Lal, D. M., Umakanth, N., Domkawale, M. A., Gopalakrishnan, V., Srivastava, M. K., and Pawar, S.: Association of Lightning with Lcl, El, Humidity at 850mb and at 200mb During Various Cape, Over Northern India, 10.2139/ssrn.4563736, 2023.

Li, H., Liu, B. M., Ma, X., Ma, Y. Y., Jin, S. K., Fan, R. N., Wang, W. Y., Fang, J., Zhao, Y. F., and Gong, W.: The Influence of Temperature Inversion on the Vertical Distribution of Aerosols, REMOTE SENSING, 14, 10.3390/rs14184428, 2022.

Li, J., Li, C. C., Guo, J. P., Li, J., Tan, W. S., Kang, L., Chen, D. D., Song, T., and Liu, L.: Retrieval of aerosol profiles by Raman lidar with dynamic determination of the lidar equation reference height, ATMOSPHERIC ENVIRONMENT, 199, 252-259, 10.1016/j.atmosenv.2018.11.048, 2019.

Li, J., Gao, W., Cao, L., Xiao, Y., Zhang, Y., Zhao, S., Liu, Z., Liu, Z., Tang, G., Ji, D., Hu, B., Song, T., He, L., Hu, M., and Wang, Y.: Significant changes in autumn and winter aerosol composition and sources in Beijing from 2012 to 2018: Effects of clean air actions, Environmental Pollution, 268, 115855, https://doi.org/10.1016/j.envpol.2020.115855, 2021.

Li, Z., Huang, Z., Bi, J., Dong, Q., Wang, Y., Abdullaev, S. F., Nozirov, D., Li, W., Li, Z., Meng, Z., Liu, W., and Song, X.: Radiative forcing and vertical heating rate of dust aerosols in southwestern Tajikistan during summer 2023, Atmospheric Environment, 345, 121051, https://doi.org/10.1016/j.atmosenv.2025.121051, 2025.

Liang, Y., Che, H., Wang, H., Zhang, W., Li, L., Zheng, Y., Gui, K., Zhang, P., and Zhang, X.: Aerosols Direct Radiative Effects Combined Ground-Based Lidar and Sun-Photometer Observations: Cases Comparison between Haze and Dust Events in Beijing, Remote Sensing, 14, 266, 2022.

Liu, S., Xing, J., Zhao, B., Wang, J., Wang, S., Zhang, X., and Ding, A.: Understanding of Aerosol–Climate Interactions in China: Aerosol Impacts on Solar Radiation, Temperature, Cloud, and Precipitation and Its Changes Under Future Climate and Emission Scenarios, Current Pollution Reports, 5, 36-51, 10.1007/s40726-019-00107-6, 2019.

Liu, S. H., Wang, H. L., Zhao, D. L., Ke, Y., Wu, Z. H., Shen, L. J., and Zhao, T. L.: Aircraft observations of aerosols and BC in autumn over Guangxi Province, China: Diurnal variation, vertical distribution and

https://doi.org/10.5194/egusphere-2026-2659
Preprint. Discussion started: 29 May 2026


source appointment, SCIENCE OF THE TOTAL ENVIRONMENT, 906, 10.1016/j.scitotenv.2023.167550, 2024.

Luo, H., Guan, Q., Shao, W., Du, Q., Xiao, X., Ni, F., and Zhang, J.: Quantifying the contribution of dust sources in the arid area of northwest China using multivariate statistical techniques and Bayesian mixing models, Journal of Cleaner Production, 379, 134672, 10.1016/j.jclepro.2022.134672, 2022.

Manavi, S. E. I., Aktypis, A., Siouti, E., Skyllakou, K., Myriokefalitakis, S., Kanakidou, M., and Pandis, S. N.: Atmospheric aerosol spatial variability: Impacts on air quality and climate change, One Earth, 8, 101237, 10.1016/j.oneear.2025.101237, 2025.

Marsli, I., Makaoui, A., Moussaoui, M., Mezrhab, A., and Diouri, M.: Analysis of aerosol optical properties and implications to radiative forcing over the Mediterranean Basin, E3S Web of Conferences, 680, 00137, 10.1051/e3sconf/202568000137, 2025.

Mazza, E. and Chen, S. S.: Compound Dry-Dusty Air Intrusions During the Genesis of Tropical Storm Kate (2021): Observations From the CPEX-AW Field Campaign and Coupled Modeling, Journal of Geophysical Research: Atmospheres, 130, e2024JD042653, https://doi.org/10.1029/2024JD042653, 2025.

Meng, L., He, Q., Zhao, T., Zhang, H., Yang, X., Mamtimin, A., Yang, F., Zhou, C., and Huo, W.: Interactions between dust aerosols and the ultra-high atmospheric boundary layer: Case study of vertical observation over the Taklimakan Desert, China, Atmospheric Environment, 343, 120977, 10.1016/j.atmosenv.2024.120977, 2025.

Nogueira, M. J. J. o. H.: Inter-comparison of ERA-5, ERA-interim and GPCP rainfall over the last 40 years: Process-based analysis of systematic and random differences, Journal of Hydrology, 583, 124632, 2020.

Noh, Y. M., Lee, H., Mueller, D., Lee, K., Shin, D., Shin, S., Choi, T. J., Choi, Y. J., and Kim, K. R.: Investigation of the diurnal pattern of the vertical distribution of pollen in the lower troposphere using LIDAR, Atmospheric Chemistry and Physics, 13, 7619-7629, 10.5194/acp-13-7619-2013, 2013.

Pace, G., Junkermann, W., Vitali, L., Di Sarra, A., Meloni, D., Cacciani, M., Cremona, G., Iannarelli, A. M., and Zanini, G.: On the complexity of the boundary layer structure and aerosol vertical distribution in the coastal Mediterranean regions: a case study, Tellus B: Chemical and Physical Meteorology, 10.3402/tellusb.v67.27721, 2015.

Pal, S., Prince, N., Anand, M., and Hamel, M.: Aerosol transport and associated boundary layer thermodynamics under contrasting synoptic conditions over a semiarid site, Science of The Total Environment, 962, 178357, 10.1016/j.scitotenv.2024.178357, 2025.

Parajuli, S. P., Stenchikov, G. L., Ukhov, A., Shevchenko, I., Dubovik, O., and Lopatin, A.: Aerosol vertical distribution and interactions with land/sea breezes over the eastern coast of the Red Sea from lidar data and high-resolution WRF-Chem simulations, ATMOSPHERIC CHEMISTRY AND PHYSICS, 20, 16089-16116, 10.5194/acp-20-16089-2020, 2020.

Park, S. and Allen, R.: Understanding influences of convective transport and removal processes on aerosol vertical distribution, Geophysical Research Letters, 42, n/a-n/a, 10.1002/2015GL066175, 2015.

Patashnick, H. and and Rupprecht, E. G.: Continuous PM-10 Measurements Using the Tapered Element Oscillating Microbalance, Journal of the Air & Waste Management Association, 41, 1079-1083, 10.1080/10473289.1991.10466903, 1991.

Peng, J.: Fine Analysis on the Rainfall Distribution of Meridional Shear Line Heavy Rain, Meteorological Monthly, 2013.

https://doi.org/10.5194/egusphere-2026-2659
Preprint. Discussion started: 29 May 2026


Petrovic, M., Radonic, J., Mihajlovic, I., Obrovski, B., Ubavin, D., M, T. S., and Miloradov, M.: Selection of optimal parameters for future research monitoring programmes on msw landfill in novi sad, Serbia, Fresenius Environmental Bulletin, 26, 4867-4875, 2017.

Prasad, P., Basha, G., and Ratnam, M. V.: Is the atmospheric boundary layer altitude or the strong thermal inversions that control the vertical extent of aerosols?, SCIENCE OF THE TOTAL ENVIRONMENT, 802, 10.1016/j.scitotenv.2021.149758, 2022.

Ramanathan, V., V. Ramana, M., Roberts, G., Kim, D., Corrigan, C., Chung, C., and Winker, D.: Warming trends in Asia amplified by brown cloud solar absorption, Nature, 448, 575-578, 10.1038/nature06019, 2007.

Reddy, K., Phanikumar, D. V., Joshi, H., Nazeer Ahammed, Y., and Naja, M.: Effect of diurnal variation of aerosols on surface reaching solar radiation, Journal of Atmospheric and Solar-Terrestrial Physics, 129, 62-68, 10.1016/j.jastp.2015.04.011, 2015.

Ricchiazzi, P., Yang, S., Gautier, C., and Sowle, D.: SBDART: A Research and Teaching Software Tool for Plane-Parallel Radiative Transfer in the Earth's Atmosphere, Bulletin of the American Meteorological Society, 79, 2101-2114, https://doi.org/10.1175/1520-0477(1998)079<2101:SARATS>2.0.CO;2, 1998.

Sarangi, C., Qian, Y., Rittger, K., Ruby Leung, L., Chand, D., Bormann, K. J., and Painter, T. H.: Dust dominates high-altitude snow darkening and melt over high-mountain Asia, Nature Climate Change, 10, 1045-1051, 10.1038/s41558-020-00909-3, 2020.

Seo, J., Kim, J. Y., Youn, D., Lee, J. Y., Kim, H., Lim, Y. B., Kim, Y., and Jin, H. C.: On the multiday haze in the Asian continental outflow: the important role of synoptic conditions combined with regional and local sources, Atmos. Chem. Phys., 17, 9311-9332, 10.5194/acp-17-9311-2017, 2017.

Serafin, S., Adler, B., Cuxart, J., De Wekker, S., Gohm, A., Grisogono, B., Kalthoff, N., Kirshbaum, D., Rotach, M., Schmidli, J., Stiperski, I., Večenaj, Ž., and Zardi, D.: Exchange Processes in the Atmospheric Boundary Layer Over Mountainous Terrain, Atmosphere, 9, 102, 10.3390/atmos9030102, 2018.

Shivkumar, G, D., E, G. K., S, P. T., R, S. K., Chate, D., and Beig, G.: Temporal variability of PM2.5 and its possible sources at the tropical megacity, Bengaluru, India, Environmental Monitoring and Assessment, 194, 10.1007/s10661-022-10235-0, 2022.

Smirnov, A., Holben, B. N., Eck, T. F., Slutsker, I., Chatenet, B., and Pinker, R. T.: Diurnal variability of aerosol optical depth observed at AERONET (Aerosol Robotic Network) sites, Geophysical Research Letters, 29, 10.1029/2002gl016305, 2002.

Song, J., Xia, X., Che, H., Wang, J., Zhang, X., and Li, X.: Daytime variation of aerosol optical depth in North China and its impact on aerosol direct radiative effects, Atmospheric Environment, 182, 31-40, 10.1016/j.atmosenv.2018.03.024, 2018.

Song, X., Zhou, T., Wang, Y., Li, X., Wu, D., Gu, Y., Lin, Z., Abdullaev, S., and Amonov, M.: Spatiotemporal evolution of dust over Tarim Basin under continuous clear-sky, Atmospheric Research, 312, 107764, 10.1016/j.atmosres.2024.107764, 2024.

Stein, A. F., Draxler, R. R., Rolph, G. D., Stunder, B. J., Cohen, M. D., and Ngan, F.: NOAA's HYSPLIT atmospheric transport and dispersion modeling system, Bulletin of the American Meteorological Society, 96, 2059-2077, 2015.

Su, B., Li, H., Zhang, M., Bilal, M., Wang, M., Atique, L., Zhang, Z., Zhang, C., Han, G., Qiu, Z., and Ali, M. A.: Optical and Physical Characteristics of Aerosol Vertical Layers over Northeastern China, Atmosphere, 11, 501, 10.3390/atmos11050501, 2020a.

Su, T., Li, Z., Li, C., Li, J., Han, W., Shen, C., Tan, W., Wei, J., and Guo, J.: The significant impact of aerosol vertical structure on lower atmosphere stability and its critical role in aerosol–planetary boundary

https://doi.org/10.5194/egusphere-2026-2659
Preprint. Discussion started: 29 May 2026


layer (PBL) interactions, Atmospheric Chemistry and Physics, 20, 3713-3724, 10.5194/acp-20-3713-2020, 2020b.

Su, T. N., Li, Z. Q., Li, C. C., Li, J., Han, W. C., Shen, C. Y., Tan, W. S., Wei, J., and Guo, J. P.: The significant impact of aerosol vertical structure on lower atmosphere stability and its critical role in aerosol-planetary boundary layer (PBL) interactions, ATMOSPHERIC CHEMISTRY AND PHYSICS, 20, 3713-3724, 10.5194/acp-20-3713-2020, 2020c.

Sun, T., Che, H., Qi, B., Wang, Y., Dong, Y., Xia, X., Wang, H., Gui, K., Zheng, Y., Zhao, H., Ma, Q., Du, R., and Zhang, X.: Aerosol optical characteristics and their vertical distributions under enhanced haze pollution events: effect of the regional transport of different aerosol types over eastern China, Atmos. Chem. Phys., 18, 2949-2971, 10.5194/acp-18-2949-2018, 2018.

Tutsak, E. and Koçak, M.: Optical and microphysical properties of the columnar Aerosol burden over the Eastern Mediterranean: Discrimination of Aerosol types, Atmospheric Environment, 229, 117463, 10.1016/j.atmosenv.2020.117463, 2020.

Valenzuela, A., Costa, M. J., Rascado, J. L., Bortoli, D., and Olmo, F.: Solar and thermal radiative effects during the 2011 extreme desert dust episode over Portugal, Atmospheric Environment, 148, 10.1016/j.atmosenv.2016.10.037, 2016.

Wang, C.-g., Xia-lu, W., Jia-de, Y., and Ting, N.: Observational study of the influences of thermal and dynamic boundary layer on the vertical distribution of black carbon aerosol in ShouXian county in wintertime, 2016, Frontiers in Earth Science, 10, 10.3389/feart.2022.1012085, 2022.

Wang, T., Li, M., Gong, M., Liu, Y., Jiang, Y., Xu, P., Ma, Y., and Sun, F.: Research on the Characteristics of Raindrop Spectrum and Its Water Vapour Transport Sources in the Southwest Vortex: A Case Study of 15–16 July 2021, Water, 16, 837, 10.3390/w16060837, 2024.

Wang, X., Liu, M., Luo, L., Chen, X., Zhang, Y., Zhang, H., Yang, S., and Li, Y.: Spatial and Temporal Distributions of Air Pollutants in Nanchang, Southeast China during 2017–2020, Atmosphere, 12, 1298, 10.3390/atmos12101298, 2021.

Wang, Y., Zhou, T., Song, X., Li, X., Wu, D., Gu, Y., Wang, J., Wei, L., Lin, Z., and Chen, R.: The Role of Nocturnal Low-Level Jets on Persistent Floating Dust over the Tarim Basin, Atmosphere, 17, 134, 2026.

Wang, Y., Yu, M., Wang, Y., Tang, G., Song, T., Zhou, P., Liu, Z., Hu, B., Ji, D., Wang, L., Zhu, X., Yan, C., Ehn, M., Gao, W., Pan, Y., Xin, J., Sun, Y., Kerminen, V.-M., Kulmala, M., and Petäjä, T.: Rapid formation of intense haze episodes via aerosol–boundary layer feedback in Beijing, Atmospheric Chemistry and Physics, 20, 45-53, 10.5194/acp-20-45-2020, 2020.

Wang, Y. H., Liu, Z. R., Zhang, J. K., Hu, B., Ji, D. S., Yu, Y. C., and Wang, Y. S.: Aerosol physicochemical properties and implications for visibility during an intense haze episode during winter in Beijing, Atmos. Chem. Phys., 15, 3205-3215, 10.5194/acp-15-3205-2015, 2015.

Wen, Q., Li, Y., Du, M., Song, W., Wei, L., Wang, Z., and Li, X.: Interdecadal shift in the impact of winter land–sea thermal contrasts on following spring transcontinental dust transport pathways in North Africa, Atmospheric Chemistry and Physics, 25, 10853-10867, 10.5194/acp-25-10853-2025, 2025.

Xiang, Y., Zhang, T. S., Liu, J. G., Wan, X., Loewen, M., Chen, X. T., Kang, S. C., Fu, Y. B., Lv, L. H., Liu, W. Q., and Cong, Z. Y.: Vertical profile of aerosols in the Himalayas revealed by lidar: New insights into their seasonal/diurnal patterns, sources, and transport*, ENVIRONMENTAL POLLUTION, 285, 10.1016/j.envpol.2021.117686, 2021.

Xie, H., Zhou, T., Fu, Q., Huang, J., Huang, Z., Jianrong, B., Shi, J., Zhang, B., and Ge, J.: Automated detection of cloud and aerosol features with SACOL micro-pulse lidar in northwest China, Optics Express, 25, 30732, 10.1364/OE.25.030732, 2017.

https://doi.org/10.5194/egusphere-2026-2659
Preprint. Discussion started: 29 May 2026


Yang, L., Zhou, T., Yang, X., Huang, Z., Wang, L., Li, X., Yang, Y., and Tao, H.: Study on a sand and dust process based on lidar network, JOURNAL OF ATMOSPHERIC AND ENVIRONMENTAL OPTICS, 20, 752-765, 2025.

Yang, X., Peng, J., Liu, B., and Liu, Y.: Multi-Scale Analysis of Grain Size in the Component Structures of Sediments Accumulated along the Desert-Loess Transition Zone of the Tengger Desert and Implications for Sources and Aeolian Dust Transportation, Atmosphere, 15, 239, 10.3390/atmos15020239, 2024.

Yim, S. H. L. and Huang, T.: Analysis of the air quality in upper atmospheric boundary layer in a high-density city in Asia using 3-year vertical profiles measured by the 3-Dimensional Real-Time Atmospheric Monitoring System (3DREAMS), Science of The Total Environment, 857, 10.1016/j.scitotenv.2022.159137, 2023.

Zhang, Q., Zhao, Y.-d., Wang, S., and Ma, F.: A Study on Atmospheric Thermal Boundary Layer Structure in Extremely Arid Desert and Gobi Region on the Clear Day in Summer , Advances in Earth Science 22 (11), 1150, 2007, 2007.

Zhang, Q., Hu, W., Ren, H., Yang, J., Deng, J., Wang, D., Sun, Y., Wang, Z., Kawamura, K., and Fu, P.: Diurnal variations in primary and secondary organic aerosols in an eastern China coastal city: The impact of land-sea breezes, Environmental Pollution, 319, 10.1016/j.envpol.2023.121016, 2023a.

Zhang, X., Zheng, Y., Che, H., Gui, K., Li, L., Zhao, H., Liang, Y., Yao, W., Zhang, X., Zhao, H., Lu, Y., and Zhang, X.: Seasonal and Diurnal Characteristics of the Vertical Profile of Aerosol Optical Properties in Urban Beijing, 2017–2021, Remote Sensing, 15, 475, 10.3390/rs15020475, 2023b.

Zhang, X. L., Zheng, Y., Che, H. Z., Gui, K., Li, L., Zhao, H. J., Liang, Y. X., Yao, W. R., Zhang, X. D., Zhao, H. H., Lu, Y. T., and Zhang, X. Y.: Seasonal and Diurnal Characteristics of the Vertical Profile of Aerosol Optical Properties in Urban Beijing, 2017-2021, REMOTE SENSING, 15, 10.3390/rs15020475, 2023c.

Zhao, C., Sun, Y., Yang, J., Li, J., Zhou, Y., Yang, Y., Fan, H., and Zhao, X.: Observational evidence and mechanisms of aerosol effects on precipitation, Science Bulletin, 69, 1569-1580, 10.1016/j.scib.2024.03.014, 2024.

Zhao, P.-j., Wu, Z., Zheng, S.-l., and Xi, S.-p.: Analysis of the Forming of Severe Convective Weather in Zhengzhou, METEOROLOGY JOURNAL OF HENAN, 2005.

Zhong, J., Zhang, X., Dong, Y., Wang, Y., Liu, C., Wang, J., Zhang, Y., and Che, H.: Feedback effects of boundary-layer meteorological factors on cumulative explosive growth of PM2.5 during winter heavy pollution episodes in Beijing from 2013 to 2016, Atmos. Chem. Phys., 18, 247-258, 10.5194/acp-18-247-2018, 2018a.

Zhong, J., Zhang, X., Dong, Y., Wang, Y., Liu, C., Wang, J., Zhang, Y., and Che, H.: Feedback effects of boundary-layer meteorological factors on cumulative explosive growth of PM <sub>2.5</sub> during winter heavy pollution episodes in Beijing from 2013 to 2016, Atmospheric Chemistry and Physics, 18, 247-258, 10.5194/acp-18-247-2018, 2018b.

Zhou, T., Xie, H., Jiang, T., Huang, J., Bi, J., Huang, Z., and Shi, J.: Seasonal characteristics of aerosol vertical structure and autumn enhancement of non-spherical particle over the semi-arid region of northwest China, Atmospheric Environment, 244, 117912, https://doi.org/10.1016/j.atmosenv.2020.117912, 2021.

Zhou, T., Xie, H., Jianrong, B., Huang, Z., Huang, J., Shi, J., Zhang, B., and Zhang, W.: Lidar Measurements of Dust Aerosols during Three Field Campaigns in 2010, 2011 and 2012 over Northwestern China, Atmosphere, 9, 10.3390/atmos9050173, 2018.

https://doi.org/10.5194/egusphere-2026-2659
Preprint. Discussion started: 29 May 2026


Zhou, T., Zhou, X., Yang, Z., Córdoba-Jabonero, C., Wang, Y., Huang, Z., Pengbo, D., Luo, Q., Zhang, Z., Shi, J., Jianrong, B., and Ali-Khodja, H.: Transboundary transport of non-east and East Asian dust observed at Dunhuang, northwest China, Atmospheric Environment, 10.1016/j.atmosenv.2023.120197, 2024.

Zhu, C.-l., Yao-ming, M. A., and Xue-long, C.: Atmospheric Boundary Layer Structure in the West and the Southeastern Periphery of the Tibetan Plateau During the Pre-Monsoon Period, Journal of Glaciology and Geocryology, 2011.